4620 *Biochemistry* **2010,** *49,* 4620–4634
DOI: 10.1021/bi9021445

BIOCHEMISTRY
including biophysical chemistry & molecular biology
*Article*

# Quantitative Characterization of the Interactions among *c-myc* Transcriptional Regulators FUSE, FBP, and FIR[†]

Hsin-hao Hsiao,[‡,§] Abhinav Nath,[§] Chi-Yen Lin,[‡] Ewa J. Folta-Stogniew,[∥] Elizabeth Rhoades,[§] and Demetrios T. Braddock*[,‡]

[‡]*Department of Pathology,* [§]*Department of Molecular Biophysics and Biochemistry, and* [∥]*W. M. Keck Biotechnology Research Laboratory, Yale University School of Medicine, New Haven, Connecticut 06520*

*Received December 14, 2009; Revised Manuscript Received April 23, 2010*

ABSTRACT: Human *c-myc* is critical for cell homeostasis and growth but is a potent oncogenic factor if improperly regulated. The *c-myc* far-upstream element (FUSE) melts into single-stranded DNA upon active transcription, and the noncoding strand FUSE recruits an activator [the FUSE-binding protein (FBP)] and a repressor [the FBP-interacting repressor (FIR)] to fine-tune *c-myc* transcription in a real-time manner. Despite detailed biological experiments describing this unique mode of transcriptional regulation, quantitative measurements of the physical constants regulating the protein−DNA interactions remain lacking. Here, we first demonstrate that the two FUSE strands adopt different conformations upon melting, with the noncoding strand DNA in an extended, linear form. FBP binds to the linear noncoding FUSE with a dissociation constant in the nanomolar range. FIR binds to FUSE more weakly, having its modest dissociation constants in the low micromolar range. FIR is monomeric under near-physiological conditions but upon binding of FUSE dimerizes into a 2:1 $FIR_2$−FUSE complex mediated by the RRMs. In the tripartite interaction, our analysis suggests a stepwise addition of FIR onto an activating FBP−FUSE complex to form a quaternary $FIR_2$−FBP−FUSE inhibitory complex. Our quantitative characterization enhances understanding of DNA strand preference and the mechanism of the stepwise complex formation in the FUSE−FBP−FIR regulatory system.

The human *c-myc* proto-oncogene is a senior administrator of cellular resources, controlling cell behaviors as diverse as proliferation, growth, differentiation, and apoptosis (*1*−*7*). Accurate levels and the timing of *c-myc* expression are extremely important for normal cell homeostasis (*8*, *9*). Multiple *cis* and *trans* elements exist for *c-myc* transcriptional regulation and are thought to form combinatorial signals to ensure that the tight regulation of *c-myc* expression is unaffected by any single factor (*10*−*12*). Among those factors, a system composed of the far-upstream element (FUSE), FUSE-binding protein (FBP), and FBP-interacting repressor (FIR) fine-tunes the *c-myc* expression level in response to the torsional stress generated as transcription progresses (Figure 1).

FUSE is a *cis* element located more than 1500 bp upstream of the *c-myc* gene and is involved in *c-myc* transcriptional regulation (*13*, *14*). FUSE contains an A/T-rich sequence (*10*, *14*) (Figure 2) and melts into single-stranded (ss) DNA in response to torsional stress generated upon transcription initiation (*14*−*16*). The noncoding strand of FUSE then recruits the *trans* activator for *c-myc* expression, FBP (*11*).

FBP selectively binds to the melted noncoding strand of FUSE and critically enhances *c-myc* transcription by stimulating the p89 helicase activity of TFIIH to drive promoter clearance of the preinitiation complex (PIC) (*17*−*21*). FBP (643 amino acids, 67473 Da) contains four K-homology (KH) motifs as its central DNA-binding domain, a predicted helix in the N-terminal thought to mediate protein−protein interactions, and a C-terminal domain that physically contacts the p89 subunit of TFIIH and is essential for its activation activity (*16*, *22*−*24*).

FIR also binds to FUSE, as well as to the central domain of FBP, and forms a stable tripartite FUSE−FBP−FIR complex, which represses activated but not basal *c-myc* transcription after transcription initiation by delaying promoter escape (*21*, *24*, *25*). FIR (542 amino acids, 58171 Da) contains two RNA recognition motifs (RRMs) (*26*), one U2AF homology motif (UHM) (*27*), and an N-terminal repression domain that binds to TFIIH and suppresses its p89/3′−5′ helicase activity (*25*). Alternative names of FIR include poly(U)-binding-splicing factor 60 kDa (PUF60) (*28*), Siah-binding protein 1 (Siah-BP1) (*29*), and Ro-binding protein 1 (RoBP1) (*30*).

FBP is critical for cellular proliferation (*16*), is developmentally regulated in mouse and chicken embryonic brain (*31*), and has been identified as a Parkin substrate (*32*). Disabling the interaction of FBP and FIR with TFIIH by mutations in the hereditary human skin cancer syndrome *xeroderma pigmentosum* primes the vulnerable *c-myc* gene for misexpression in neoplasia (*21*). A splice variant of FIR lacking the repression domain was identified in human colorectal cancers, underscoring FIR's role in *c-myc* regulation (*33*). Both FBP and FIR are targets for the development of cancer diagnosis and therapy (*34*, *35*). FIR, alternatively known as PUF60, also possesses pre-mRNA splicing activity (*28*).

In the FUSE−FBP−FIR system, DNA topology is thought to play an essential role in transcriptional regulation (*14*). Not only can FUSE melt into ssDNA upon transcription initiation, but the

[†]Funding for this project has been provided by American Cancer Society Grant RSG-0-222-01 to D.T.B. H.H. was supported by the Anna Fuller Fellowship in Molecular Oncology.

*To whom correspondence should be addressed: Department of Pathology, Yale University School of Medicine, 310 Cedar St., LH404, New Haven, CT 06510. Telephone: (203) 737-1278. Fax: (203) 785-6899. E-mail: demetrios.braddock@yale.edu.

 Published on Web 04/26/2010 

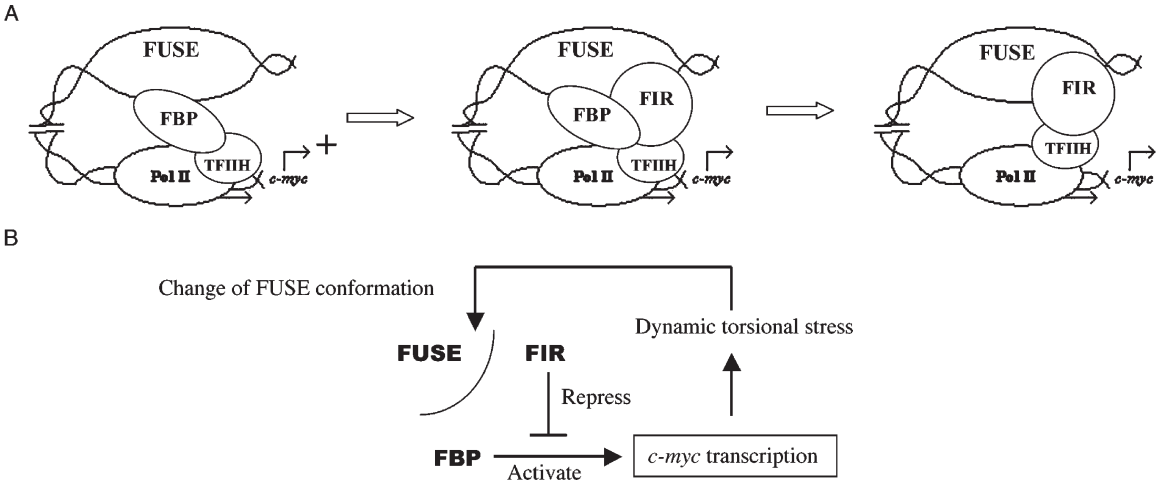


FIGURE 1: Current models for the involvement of FUSE, FBP, and FIR in the transcriptional regulation of *c-myc*. (A) Stepwise complex formation of FUSE, FBP, and FIR in the transcriptional regulation of *c-myc*. In step 1, melting of FUSE allows its noncoding strand to recruit FBP for activating *c-myc* transcription. The C-terminal activation domain of FBP has physical contact with TFIIH to upregulate its helicase activity. In step 2, FIR joins the FBP−FUSE complex to form a tripartite inhibitory complex, suppressing the activation effect of FBP and bringing *c-myc* transcription back to basal levels. FIR also physically contacts TFIIH. In step 3, in the later stage of the regulatory event, FBP is removed from FUSE, while FIR remains on FUSE for an extended period of time. (B) Schematic representation of the functional coordination among FUSE, FBP, and FIR.

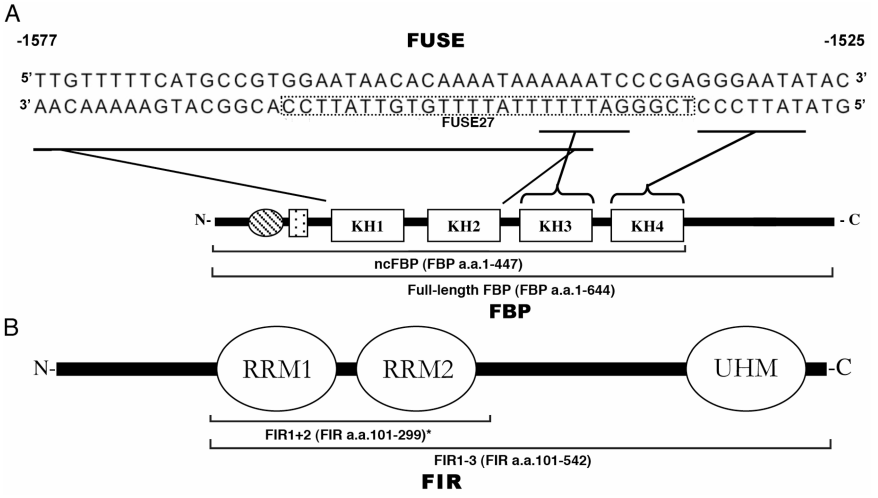


FIGURE 2: Sequence of FUSE and domain structures of FBP and FIR. (A) The top panel shows the sequence of the far-upstream sequence element (FUSE) DNA (*10*). The lower strand is the noncoding strand of FUSE; the dotted rectangular box indicates the sequence of FUSE27, a 27-mer region for FIR interaction. The bottom panel shows the domain structure of the FUSE-binding protein (FBP). FBP has four K-homology motifs (KH1−4), which are used for both nucleic acid binding and protein−protein association with FIR. Extended solid lines indicate the corresponding FUSE sequences that interact with the FBP KHs. The C-terminus of FBP is its activation domain, which has physical contacts with TFIIH during the regulation. The hatched oval indicates a glycine-rich region. The dotted rectangle denotes a predicted helix that is critical for protein−protein interaction with FIR (*18*, *23*, *24*). Two constructs [full-length FBP (FBP amino acids 1−644) and ncFBP (FBP amino acids 1−447)] were used in this study. (B) FIR is a 542-amino acid protein at full length, consisting of a N-terminal repression domain, two RNA recognition motifs (RRMs), and one U2AF homology motif (UHM). The FIR construct used in this study is FIR1−3 (FIR amino acids 101−542), which consists of both FIR's RRMs and UHM. FIR1+2 (FIR amino acids 101−299), which consists of only FIR's two RRMs but not the UHM, is a construct used in our previously study of FIR (*43*) and is listed to facilitate comparison and discussion of FIR's domain function.

torsional stress generated during transcription may continuously modulate the chromatin structure to mechanically monitor the progress of transcription in a real-time manner (*11*, *15*, *16*, *36*, *37*). The structural transitions of ssFUSE may actively involve and/or be exploited by FBP and FIR in the performance of their regulating functions during the transcription as we know that activities of FBP and FIR are both FUSE-dependent (*17*, *25*).

Overall, the FUSE−FBP−FIR and TFIIH system presents an example of a remote *cis* element (FUSE) that uses the conformational change of the target site (melted, ssDNA) to monitor the progression of gene transcription (*c-myc*) and to recruit *trans* effectors (FBP and FIR) that influence the general transcription complex (TFIIH helicase activity) (Figure 1) (*21*, *38*, *39*). This is a highly unique mode of transcriptional regulation that has been suggested to be broadly relevant to eukaryotic gene transcription (*38*, *40*, *41*).

The structural basis for the FUSE−FBP−FIR system has been partially enlightened by the structures of the individual domains of FBP and FIR in complex with FUSE (*42*, *43*). Solution dynamics between two FBP KH motifs suggests FBP binds to FUSE in an extended and linear pattern (*42*); this conclusion is verified by testing different sequences for optimal binding with FBP (*44*).

Dimerization of FIR RRMs onto the FUSE strand is proposed to modulate FUSE conformation and is implicated in the ejection of FBP from FUSE (*43*).

Here we investigate the biochemical and solution properties of the protein−DNA interactions among FBP, FIR, and FUSE. We provide a conformational and quantitative basis for understanding the DNA strand preference and the order of complex formation in the FUSE−FBP−FIR system. Our analysis also suggests the requirement of an additional energetic contribution in the cell for driving the transition of stepwise complex formation in this unique mechanism of transcriptional control of the *c-myc* proto-oncogene.

## MATERIALS AND METHODS

*Preparation of Protein and DNA Constructs*. Nucleotides encoding human far-upstream element (FUSE)-binding protein (FBP) (UniProtKB/Swiss-Prot entry Q96AE4) amino acids 1−644 cloned in pFastBac HT B (Invitrogen) were kindly provided by the David Levens Group (National Cancer Institute, Bethesda, MD). Cloning artifacts introduced 69 amino acids at the N-terminus of the protein (MSYYHHHHHHDYDIPTTENLYFQGAMGSGIERPTSTSSLVTAASVLEFCRSSGSPIEFRLRGSGSYSAT). This protein is hereafter termed full-length FBP. Full-length FBP was expressed as a protein with a molecular mass of 75179.7 Da with the baculoviral expression system in insect cell strain Sf21. This full-length FBP construct was previously used by Benjamin *et al.* (*44*). A previous study by Duncan *et al.* (*17*), who found comparable binding properties for the purified human FBP and the N-terminally GST-fused recombinant FBP, gave us confidence that the extraneous N-terminal residues do not significantly influence the *in vitro* DNA binding behavior of FBP.

The C-terminal activation domain of FBP was suspected to cause nonspecific association with the Superdex S-200 resin. Therefore, a FBP C-terminally truncated construct with nucleotides encoding FBP amino acids 1−447 (hereafter termed ncFBP) was cloned in the pET100 protein expression vector with the Champion pET Directional TOPO Expression System (Invitrogen). Cloning artifacts introduced 43 amino acids at the N-terminus of the protein (MRGSHHHHHHGMASMTGGQQMGRDLYDDDDKDHPFTENLYFQG). To ease protein handling, cysteines 132, 148, and 332 were replaced with alanines with the QuickChange site-directed mutagenesis kit (Stratagene, La Jolla, CA). ncFBP was expressed in *Escherichia coli* strain BL21(DE3), using standard methods. ncFBP has a molecular mass of 52111.3 Da.

Nucleotides encoding human FBP-interacting repressor (FIR) (UniProtKB/Swiss-Prot entry Q9UHX1-2) amino acids 101−542 (hereafter termed FIR1−3) were cloned into the pET100 protein expression vector. Cloning artifacts introduced four amino acids (GRGS) at the N-terminus of the protein following cleavage of a histidine tag with TEV protease. To ease protein handling, cysteine residues in the FIR sequence were replaced with serine (Cys112) or alanine (Cys238 and Cys470) depending on their predicted location in the protein structure (alanine if buried, serine if exposed). The proteins were expressed in *E. coli* strain BL21(DE3), using standard methods. FIR1−3 has a molecular mass of 47970.7 Da.

Synthetic FUSE DNA sequences of the noncoding strand 53-mer (5′-GTATATTCCCTCGGGATTTTTTATTTTGTGTTATTCCACGGCATGAAAAACAA-3′, hereafter termed FUSE53) (*10*), 27-mer (5′-TCGGGATTTTTTATTTTGTGTTATTCC-3′, FUSE27), and the coding strand 53-mer (5′-TTGTTTTTCATGCCGTGGAATAACACAAAATAAAAAATCCCGAGGGAATATAC-3′, codingFUSE53) were purchased from The Midland Certified Reagent Co. (Midland, TX).

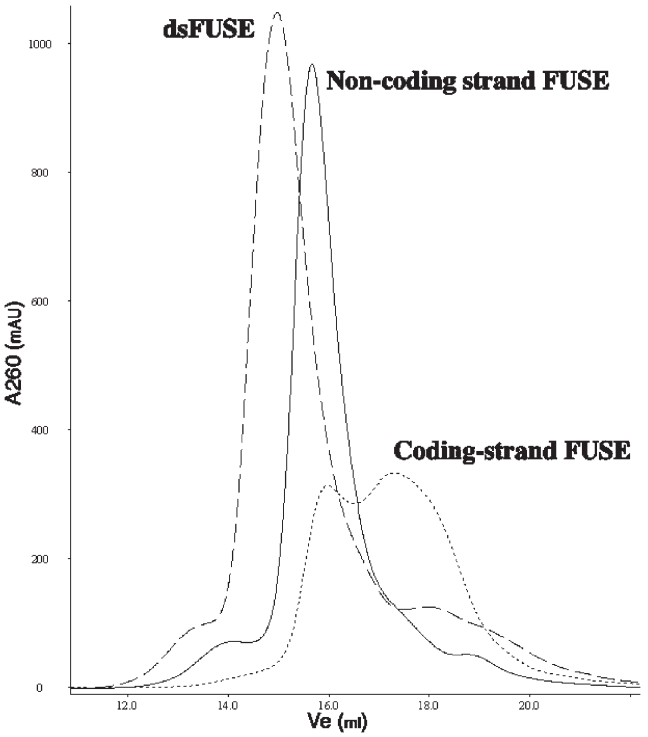


FIGURE 3: Coding and noncoding strands of FUSE adopt different conformations as single-stranded DNA. The elution profiles of the coding and noncoding strands of FUSE (3 nmol in 200 $\mu$L injections) were analyzed by size-exclusion chromatography (Superdex S-200, 10/30, GL SEC column). Elution traces were followed by their absorption at 260 nm. A more compact conformation of the coding strand is detected by the presence of a second peak at an elution volume of 17.29 mL with an $r_S$ of 22.9 Å and an apparent molecular mass of 14.9 kDa. In contrast, the noncoding strand elutes at 15.66 mL with an estimated hydrodynamic radius of 33.2 Å and an apparent molecular mass of 37.4 kDa, compared to its sequence-predicted molecular mass of 16.3 kDa, suggesting that the noncoding strand maintains an extended conformation when unwound into single-stranded DNA.

*Analytical Size-Exclusion Chromatography*. Analytical size-exclusion chromatography (SEC) was performed in an eluent buffer that consisted of 50 mM Tris-HCl, 150 mM NaCl, and 20 $\mu$M EDTA (pH 8.0) at a flow rate of 1 mL/min, with a Superdex S-200, 10/30, GL SEC column, connected to the ÄKTA Purifier FPLC system (Amersham Biosciences, GE Healthcare, Piscataway, NJ). Elution peaks were spectrophotometrically monitored by their absorption at 280 and 260 nm. The volumes of the eluent from the point of application to the center of the elution peaks were measured to determine the void volume ($V_o$) with the injection of 500 $\mu$L of Blue Dextran 2000 at a concentration of 1 mg/mL and the elution volume ($V_e$) with the injection of protein standards and samples. A standard calibration curve was obtained by plotting the logarithms of the known molecular masses of protein standards versus their respective $V_e/V_o$ values. Protein standards used for calibration include 70 $\mu$L of bovine albumin (67000 Da, 35.5 Å, 10 mg/mL) supplied in the low molecular weight gel filtration calibration kit (Amersham Biosciences, GE Healthcare) and 120 $\mu$L of the Bio-Rad Gel Filtration Standard consisting of bovine thyroglobulin (670000 Da, pI 4.5, 10 mg/mL, 85.0 Å),

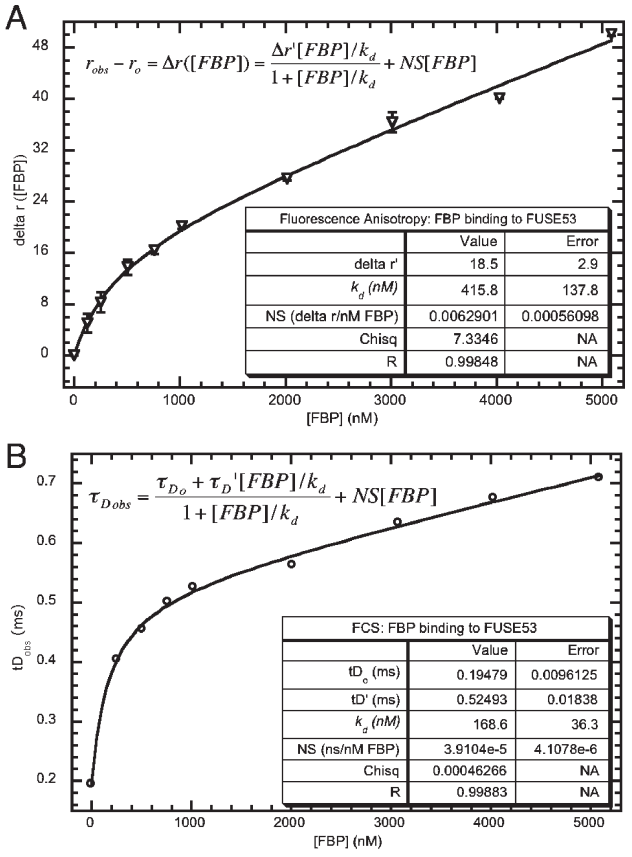


FIGURE 4: FBP binds to noncoding strand FUSE with a dissociation constant in the low nanomolar range. Fluorescein-labeled FUSE53 (10 nM) was mixed with increasing concentrations of flFBP and incubated at room temperature for 30 min before the measurement. (A) FBP−FUSE binding affinity based on fluorescence anisotropy (FA). The binding curve is fitted with the listed equation assuming 1:1 stoichiometry. After a linear, nonspecific phase is deconvoluted, the $k_d$ is estimated to be 415.8 ± 137.8 nM. (B) FBP−FUSE binding affinity based on fluorescence correlation spectroscopy (FCS). A $k_d$ of 168.6 ± 36.3 nM is derived. Both FA and FCS reported a high affinity between FBP and FUSE53 with a $k_d$ in the low nanomolar range.

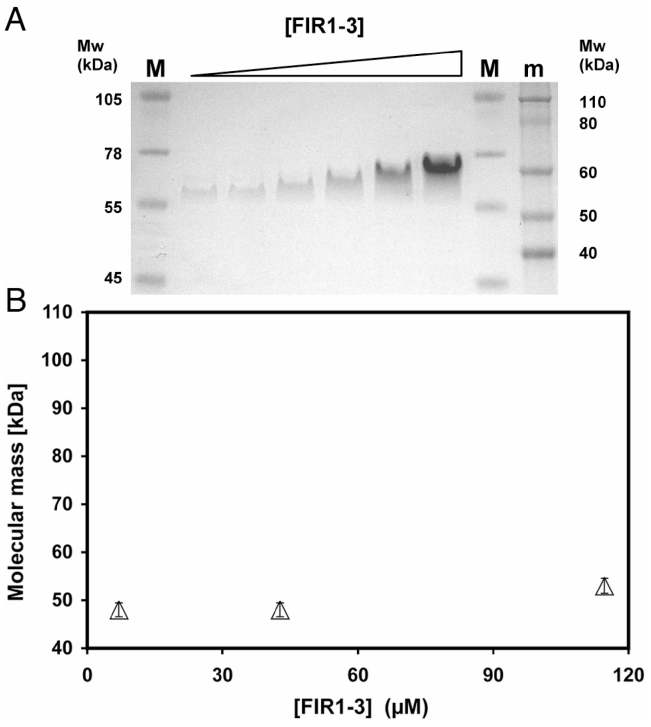


FIGURE 5: FIR1−3 shows SDS-resistant oligomerization but is monomeric under a near-physiological condition. (A) SDS−PAGE analysis of FIR1−3, with serial 2-fold dilution starting from 9.5 μM, shows that FIR1−3 forms concentration-dependent and SDS-resistant oligomerization under non-native conditions. Lane M contained SeeBlue Plus2 Pre-Stained Standard (Invitrogen), and lane m contained Novex Sharp Prestained Protein Standard (Invitrogen). The molecular masses of standard proteins are labeled. (B) Static light scattering demonstrates that FIR assumes a monomeric conformation under physiological conditions. Each triangle denotes an average molecular mass determined by static light scattering readings at a certain FIR1−3 concentration.

bovine γ-globulin (158000 Da, pI 5.1, 10 mg/mL, 53.4 Å), chicken ovalbumin (44000 Da, pI 4.6, 10 mg/mL, 30.5 Å), equine myoglobin (17000 Da, pI 6.9, 5 mg/mL, 20.5 Å), and vitamin $B_{12}$ (1350 Da, pI 4.5, 1 mg/mL, 1.6 Å). Vitamin $B_{12}$ was detected by $A_{361}$. The partition coefficient ($K_{av}$) was determined with the equation $K_{av} = (V_e - V_o)/(V_t - V_o)$, where $V_t$ is the total bed volume. Known Stokes radii ($r_S$) of standard proteins were plotted against $(-\log K_{av})^{1/2}$ for the estimation of the $r_S$ of samples. Experimental $V_e$ values obtained on different columns were normalized in reference to the relative $V_e$ values of FUSE53.

For studying the FUSE DNA, 3 nmol of the 53-mer noncoding or coding strand of FUSE or 1.5 nmol of 53 bp double-stranded FUSE was applied to the SEC column in 200 μL injections.

For studying the FBP−FIR protein−protein interaction, 8.3 nmol of ncFBP, 66.6 nmol of FIR1−3, or their mixture was incubated at room temperature for 30 min before being subjected to a 500 μL injection on the SEC column.

*SDS−PAGE.* For Figure 5, reaction mixtures of 8 μL of Novex Tricine SDS Sample Buffer (2×) (Invitrogen) and 8 μL of protein samples at the designated final concentrations were heated at 94 °C for 10 min and cooled at room temperature for 10 min before 15 μL of the reaction mixture was loaded onto a Novex 10% Tricine Gel (1.0 mm, 12 wells) (Invitrogen). For Figure 8, reaction mixtures of 4 μL of NuPAGE LDS Sample Buffer (4×) (Invitrogen) and 12 μL of protein samples were heated at 94 °C for 5−8 min and cooled at room temperature before 16 μL of the reaction mixture was loaded onto a 4 to 12% BisTris NuPAGE mini-gel (1.0 mm, 12 wells) (Invitrogen) in MOPS buffer. Five microliters of SeeBlue Plus2 Pre-Stained Standard (Invitrogen) and/or Novex Sharp Prestained Protein Standard (Invitrogen) was subjected to electrophoresis along the samples to denote the apparent molecular masses. Electrophoresis was performed as suggested by the gel system supplier.

*Fluorescence Anisotropy (FA) Analysis.* Binding of FBP and FIR to the FUSE DNA was monitored by a change in the steady-state fluorescence anisotropy ($r$) of a fluorescein-labeled FUSE53 (*5′-GTATATTCCCTCGGGATTTTTATTTTGTGTTATT-CCACGGCATGAAAAACAA-3′, *FUSE53) and FUSE27 (5′-TCGGGATTTTTTATTTTGTGTTATTCC-3′*, *FUSE27). Experiments were conducted in 50 mM Tris-HCl, 150 mM NaCl, and 20 μM EDTA (pH 8). When full- length FBP was studied, additional 1 mM DTT was included in the buffer. The concentration of labeled FUSE was kept constant at 10 nM, while the concentration of protein was varied from 0 to 200 μM. Samples were equilibrated at room temperature for at least 30 min before measurements were taken on an EnVision Multilabel Plate Reader (model 2101, PerkinElmer, Waltham, MA). Reaction

mixtures were excited with a 480 nm polarized filter, and the emission was read with two 535 nm polarized filters, one parallel to the polarization of the excitation filter and the other perpendicular.

The observed anisotropy ($r_{obs}$) is calculated with the equation $r_{obs} = 1000(I_{||} - GI_{\perp})/(I_{||} + 2GI_{\perp})$, where $I_{||}$ and $I_{\perp}$ are the background-subtracted fluorescence count rates of the emission parallel ($I_{||}$) and perpendicular ($I_{\perp}$) to the excitation plane, respectively, and the $G$ (grating) factor is an instrument- and assay-dependent correction factor.

Equilibrium binding affinities were obtained by fitting the [FBP]- or [FIR]-dependent change in anisotropy [$\Delta r$([FBP]) or $\Delta r$([FIR])] to the following equations. For FBP-FUSE binding, equation 1 assumes one FBP molecule binds to one FUSE molecule:

$$r_{obs} - r_o = \Delta r([FBP]) = \frac{\Delta r'[FBP]/k_d}{1 + [FBP]/k_d} + NS[FBP] \quad (1)$$

where $r_o$ is the anisotropy of free *FUSE, $\Delta r'$ is the difference between $r_o$ and the anisotropy of one FBP molecule specifically bound to *FUSE, $k_d$ is the specific equilibrium dissociation constant for the one FBP binding to *FUSE, and NS is the slope of a linear term included to account for weak nonspecific binding between FBP and *FUSE.

For FIR-FUSE binding, equation 2 assumes that two FIR molecules bind to two independent sites on the labeled FUSE:

$$r_{obs} - r_o = \Delta r([FIR]) = \frac{\Delta r_1[FIR]/k_{d1} + \Delta r_2[FIR]^2/(k_{d1}k_{d2})}{1 + [FIR]/k_{d1} + [FIR]^2/(k_{d1}k_{d2})} \quad (2)$$

where $\Delta r_1$ is the difference between $r_o$ and the anisotropy of one FIR molecule bound to *FUSE, $\Delta r_2$ is the difference between $r_o$ and the anisotropy of two FIR molecules bound to *FUSE, $k_{d1}$ is the equilibrium dissociation constant for the first FIR binding to *FUSE, and $k_{d2}$ is the equilibrium dissociation constant for the second FIR binding to *FUSE (for a detailed description of the derivation of the equation, please see the Supporting Information).

For the FUSE, FBP, FIR tripartite interaction, equilibrium binding affinities were obtained by fitting the [FBP]- and [FIR]-dependent change in anisotropy [$\Delta r$([FBP],[FIR])] to two nested but different models. Model 1 assumes only one FIR molecule is present in the tripartite FUSE−FBP−FIR complex, as demonstrated by the following equation (eq 3):

$$\begin{aligned} r_{obs} - r_o &= \Delta r([FBP],[FIR]) \\ &= [\Delta r'([FBP])/k_d + \Delta r_1([FIR])/k_{d1} \\ &+ \Delta r_2([FIR])^2/(k_{d1}k_{d2}) + \Delta r_{FUSE-FBP-FIR}[FBP][FIR]/ \\ &(k_d k_{d,FUSE-FBP-FIR})]/[1 + [FBP]/k_d + [FIR]/k_{d1} \\ &+ [FIR]^2/(k_{d1}k_{d2}) + [FBP][FIR]/(k_d k_{d,FUSE-FBP-FIR})] \\ &+ NS[FBP] \end{aligned} \quad (3)$$

where $\Delta r_{FUSE-FBP-FIR}$ is the difference between $r_o$ and the anisotropy of one FIR molecule bound to the *FUSE−FBP binary complex and $k_{d,FUSE-FBP-FIR}$ is the equilibrium dissociation constant for the one FIR molecule binding to *FUSE.

Model 2 assumes that two FIR molecules can bind to the *FUSE−FBP binary complex, as demonstrated by the following equation (eq 4):

$$\begin{aligned} r_{obs} - r_o &= \Delta r([FBP],[FIR]) \\ &= [\Delta r'([FBP])/k_d + \Delta r_1([FIR])/k_{d1} + \Delta r_2([FIR])^2 \\ &/(k_{d1}k_{d2}) + \Delta r_{FUSE-FBP-2FIR}[FBP][FIR]/ \\ &(k_d k_{d,FUSE-FBP-FIR}) + \Delta r_{FUSE-FBP-2FIR}[FBP][FIR]^2/ \\ &(k_d k_{d,FUSE-FBP-FIR} k_{d,FUSE-FBP-2FIR})]/[1 + [FBP]/k_d \\ &+ [FIR]/k_{d1} + [FIR]^2/(k_{d1}k_{d2}) + [FBP][FIR]/ \\ &(k_d k_{d,FUSE-FBP-FIR}) + [FBP][FIR]^2/ \\ &(k_d k_{d,FUSE-FBP-FIR} k_{d,FUSE-FBP-2FIR})] + NS[FBP] \end{aligned} \quad (4)$$

where $\Delta r_{FUSE-FBP-2FIR}$ is the difference between $r_o$ and the anisotropy of two FIR molecules bound to the *FUSE−FBP binary complex and $k_{d,FUSE:FBP:2FIR}$ is the equilibrium dissociation constant for the second FIR molecule binding to the *FUSE−FBP complex. In models 1 and 2, values for $\Delta r'$, $k_d$, $\Delta r_1$, $\Delta r_2$, $k_{d1}$, and $k_{d2}$ are directly inserted with the results obtained in Figure 4A and Figure 7B. All the curve fitting in this study was performed with KaleidaGraph version 4.03 (Synergy Software, Reading, PA).

*Fluorescence Correlation Spectroscopy* (*FCS*). Experiments were conducted in 50 mM Tris-HCl, 150 mM NaCl, 20 $\mu$M EDTA (pH 8), and 1 mM DTT. The concentration of labeled FUSE was kept constant at 10 nM, while the concentration of protein was varied. FCS data were collected on a lab-built instrument based on an Olympus IX-71 inverted microscope (Olympus America, Center Valley, PA) equipped with a 60×/1.2 N.A. water objective. The sample was illuminated with a 488 nm, 50 mW diode-pumped solid-state continuous-wave laser (Coherent, Santa Clara, CA), adjusted with neutral density filters to ~5 $\mu$W measured power just prior to entry into the microscope. Fluorescence was collected through a 575/150 band-pass filter (Chroma, Rockingham, VT), coupled through a 50 $\mu$m diameter optical fiber (Oz Optics, Ottawa, ON, Canada) to an avalanche photodiode (PerkinElmer), and autocorrelated using a FLEX03-LQ-12 correlator (Correlator.com, Bridgewater, NJ).

Thirty 10 s autocorrelation traces were collected for each sample. If necessary, a small number of traces containing obvious artifacts caused by slowly diffusing aggregates or contaminant particles were discarded. The remaining traces were averaged and fit to the following autocorrelation decay equation:

$$G(\tau) = \frac{1}{N}\left(1 + \frac{\tau}{\tau_D}\right)^{-1}\left(1 + \frac{\tau}{s^2\tau_D}\right)^{-1/2} \quad (5)$$

where $G(\tau)$ is the autocorrelation as a function of time $\tau$, $N$ is the average number of labeled particles in the focal volume, $\tau_D$ is the mean characteristic diffusion time of labeled particles, and $s$ is the ratio of the axial to radial dimensions of the observation volume. The autocorrelation curves were also analyzed with a multicomponent fit which yields the relative fractions of *FUSE−FBP complex and free *FUSE; however, the $K_D$ values determined from this analysis were comparable to those extracted from plotting the mean $\tau_D$, and thus, we chose to use this parameter ($\tau_D$) for the sake of simplicity.

Equilibrium binding affinities were obtained by fitting the observed [FBP]-dependent diffusion time ($\tau_{D,obs}$) to the following

equation, assuming one FBP molecule binds to one FUSE molecule:

$$\tau_{D,obs} = \frac{\tau_{D,o} + \tau_D'[FBP]/k_d}{1 + [FBP]/k_d} + NS[FBP] \quad (6)$$

where $\tau_{D,o}$ is the diffusion time of free *FUSE, $\tau_D'$ is the diffusion time of the specifically bound *FUSE−FBP complex, $k_d$ is the specific equilibrium dissociation constant for the one FBP binding to *FUSE, and NS is the slope of a linear term included to account for weak nonspecific binding between FBP and *FUSE.

*Size-Exclusion Chromatography-Coupled Laser Light Scattering* (*SEC-LS*). The light scattering data were collected using a Superdex 200, 10/30, HR SEC column (GE Healthcare), connected to a high-performance liquid chromatography system (HPLC), Agilent 1200 (Agilent Technologies, Wilmington, DE), equipped with an autosampler. The elution from SEC was monitored by a photodiode array (PDA) UV−vis detector, UV (Agilent Technologies), a differential refractometer, RI (OPTI-Lab rEx Wyatt Corp., Santa Barbara, CA), a static and dynamic multiangle laser light scattering (LS) detector (HELEOS II with QELS capability, Wyatt Corp.). The SEC-UV/LS/RI system was equilibrated in 50 mM Tris-HCl, 150 mM NaCl, and 20 $\mu$M EDTA (pH 8.0) at a flow rate of 1.0 mL/min. Two software packages were used for data collection and analysis: Chemstation (Agilent Technologies) controlled the HPLC operation and data collection from the multiwavelength UV−vis detector, while ASTRA (Wyatt Corp.) collected data from the refractive index detector and the light scattering detectors and recorded the UV trace at 280, 295, or 315 nm sent from the PDA detector. The weight-average molecular weights ($M_w$) were determined across the entire elution profile in intervals of 1 s from static LS measurement using ASTRA as previously described (*45*).

*Isothermal Titration Calorimetry* (*ITC*). The heats generated by addition of FIR1−3 to ncFBP in a sample cell were measured at 30 °C using a VPITC calorimeter (Microcal, Piscataway, NJ). Samples were extensively dialyzed into 50 mM NaCl and 25 mM Hepes (pH 7.4) before the experiments; 6.4 $\mu$M ncFBP was placed in the sample cell, and 124.4 $\mu$M FIR1−3 was injected into the cell through the syringe. Reference experiments were performed with FIR1−3 injected into buffer, buffer injected into ncFBP, and buffer injected into buffer. Data were processed with Origin version 5.0 (Microcal).

*Statistical Analysis*. Model 1 is designated as the null hypothesis and model 2 as the alternative hypothesis. Since models 1 and 2 are nested equations, we could compare the quality of fit of the two models with both the corrected Akaike's Information Criteria (AICc) method and the *F*-test. Both tests are performed with the QuickCalcs online tool provided by GraphPad Software (La Jolla, CA).

## RESULTS

*Different Conformations of FUSE Coding and Noncoding Strands*. Upon active transcription, FUSE on the chromatin melts into single-stranded DNA, thus making its noncoding strand available for interaction with FBP. To study the solution conformations of both FUSE strands in their full-length context, we subjected 53-mer oligonucleotides representing the sequences of the coding and noncoding strand FUSE as well as their annealed FUSE duplex to analytical size-exclusion chromatography (SEC) (Figure 3). We found that while the noncoding strand of FUSE (hereafter termed FUSE53) shows only one major conformation in solution with an apparent molecular mass of 37.4 kDa (230% of its sequence-predicted mass of 16.3 kDa), the coding strand of FUSE is heterogeneous with at least two separate conformations: an extended conformation (apparent molecular mass of 31.4 kDa) similar to that of FUSE53 and a second population that is more compact as determined by a later elution profile with an apparent molecular mass of 14.9 kDa (91% of its predicted molecular mass of 16.3 kDa) (Table 1). This result suggests that the coding strand of FUSE has the propensity to adopt secondary or tertiary structure as a single strand, while the noncoding strand maintains an extended conformation.

Table 1: SEC-Based Peak Analysis of FUSE DNA

| peak $V_e$[a] (mL) | assignment | predicted molecular mass (kDa) | apparent molecular mass (kDa) | estimated $r_S$[b] (Å) |
|---|---|---|---|---|
| 14.25 | dsFUSE | 32.6 | 55.2 | 37.8 |
| 15.66 | FUSE53 | 16.3 | 37.4 | 33.2 |
| 15.97 | coding FUSE | 16.3 | 31.4 | 31.2 |
| 17.29 | coding FUSE | 16.3 | 14.9 | 22.9 |

[a]Raw data drawn from analytical SEC-based analysis in Figure 3. [b]$r_S$, Stokes radius.

*FBP Binds to Noncoding FUSE with a Dissociation Constant in the Nanomolar Range*. To study the equilibrium binding affinity between FBP and FUSE, we mixed 10 nM fluorescein-labeled FUSE53 with increasing concentrations of full-length FBP, incubated the reaction mixtures at room temperature for 30 min, and measured their fluorescence anisotropy (Figure 4A). The binding curve for FBP and FUSE has a linear phase at higher FBP concentrations, consistent with nonspecific association at higher concentrations of protein. Using the method, we estimated the $k_d$ between FBP and FUSE to be in the nanomolar range (415.82 ± 137.8 nM).

To cross-validate this binding affinity, we repeated the experiment with an alternative technique, fluorescence correlation spectroscopy (FCS), which detects the translational movement of fluorescein-labeled DNA (Figure 4B). In FCS, the fluctuations in fluorescence from a dilute solution of labeled molecules or complexes diffusing through a small focal volume are autocorrelated. The time scale of autocorrelation decay is determined by the rates of any processes that affect the fluorescent signal, including diffusion of particles into and out of the ~1 fL focal volume. Fluorescein-labeled FUSE53 (10 nM) was mixed with increasing concentrations of full-length FBP and incubated at room temperature for 30 min before the correlated diffusion time ($\tau_D$) was measured. The FCS-estimated equilibrium dissociation constant for FBP and FUSE was 168.55 ± 36.326 nM, which is comparable to the estimate using fluorescence anisotropy.

*Although Apo-FIR1−3 Appears To Be Oligomerizing on SDS−PAGE, It Is Predominantly Monomeric in Solution up to 115 $\mu$M*. Apo-FIR was previously characterized by analytical ultracentrifugation to be mostly monomeric, though with wide dispersity, at 11 $\mu$M in solution (*46*). To further clarify the solution conformation of both apo-FIR and the FIR−DNA complex over a wide concentration range, we studied a FIR construct consisting of both of the two RRMs and the UHM of FIR, in which construct we mutated its cysteines to serine (Cys112 in RRM1) or alanine (Cys238 in RRM2 and Cys470 in UHM) to improve protein stability (hereafter termed FIR1−3). In SDS−PAGE analysis, apo-FIR1−3 appears to undergo significant

concentration-dependent continuous molecular mass shift (Figure 5A), which is reminiscent of the unusual behavior previously observed for FIR in forming a dimer upon SDS−PAGE (*28*, *46*) (see the Supporting Information). However, when analyzed by size-exclusion chromatography-coupled light scattering (SEC-LS) under a near-physiological condition, apo-FIR1−3 was almost entirely monomeric in solution with a weak tendency to aggregate above 100 $\mu$M (Figure 5B). This suggests the monomer is the physiologically relevant conformation of apo-FIR.

*FUSE Binding Induces FIR Dimerization*. To study the conformations of FIR in complex with FUSE, we used SEC-LS to analyze a mixture of FIR1−3 with excess 27-mer noncoding strand FUSE sequence (FUSE27) (FUSE27:FIR1−3 molar ratio of > 1.1), which has been demonstrated to be sufficient to interact with FIR (*43*). Experiments were conducted under identical near-physiological conditions as for the apo-FIR. We found that FUSE DNA induced the dimerization of FIR1−3 (Figure 6A). The stoichiometry of the FUSE27:FIR1−3 complex was derived from UV:RI ratios (Figure 6B), which supports a single strand of DNA interacting with a dimer of FIR.

*FIR Binds to the Noncoding Strand of FUSE More Weakly Than FBP, with Dissociation Constants in the Micromolar Range*. To study the equilibrium binding affinity of FIR and FUSE, we mixed 10 nM fluorescein-labeled FUSE27 with increasing concentrations of FIR1−3. Reaction mixtures were incubated at room temperature for 30 min before their fluorescence anisotropy was measured (Figure 7A). The binding curve for FIR1−3 and FUSE27 was fit to a two-site binding model. The affinities between FIR1−3 and FUSE27 are in the micromolar range ($k_{d1} = 0.6 \pm 0.3$ $\mu$M; $k_{d2} = 20.9 \pm 6.4$ $\mu$M).

The binding affinity of FIR1−3 with the entire FUSE sequence (FUSE53) was also examined under identical conditions (Figure 7B), yielding similar dissociation constants in the low micromolar range ($k_{d1} = 3.3 \pm 0.5$ $\mu$M; $k_{d2} = 97.8 \pm 42.3$ $\mu$M). These experiments demonstrate that FIR has a weaker affinity for FUSE than FBP.

*FIR−FBP Protein−Protein Interaction*. FBP and FIR have been reported to associate in the absence of DNA (*24*). To further characterize this behavior, we studied the protein interactions by analytical size-exclusion chromatography (SEC) and isothermal titration calorimetry (ITC) (Figure 8).

ncFBP (8.3 nmol), FIR1−3 (66.6 nmol), or their mixture was applied to the analytical SEC column (Figure 8A). We first found that both ncFBP and FIR1−3 may adopt nonglobular conformations in solution. ncFBP has a hydrodynamic radius of 42.7 Å and an apparent molecular mass of 82840.1 Da (159% of its predicted mass of 52111.3 Da). FIR1−3 has an estimated hydrodynamic radius of 46.8 Å and an apparent molecular mass of 113584.8 Da (237% of its predicted mass of 47970.7 Da) (Table 2). The ncFBP−FIR1−3 mixture generated an additional absorption peak with an earlier elution volume of 13.00 mL. SDS−PAGE verified that ncFBP and FIR1−3 coelute in this additional peak (fraction A12), consistent with the ncFBP−FIR1−3 complex (Figure 8B). The ncFBP−FIR1−3 complex has an estimated hydrodynamic radius of 52.1 Å and an apparent molecular mass of 167580.0 Da (167% of its predicted mass of 100082.0 Da, assuming 1:1 stoichiometry) (Table 2), suggesting that the complex formed by the two proteins also deviates from the globular form.

By ITC analysis (Figure 8C), we qualitatively confirmed the interactions between FBP and FIR, but their affinity could not be confidently measured because of the weak affinity and low heat of generation but is estimated from the data to be weaker than the affinity of either protein for ssDNA.

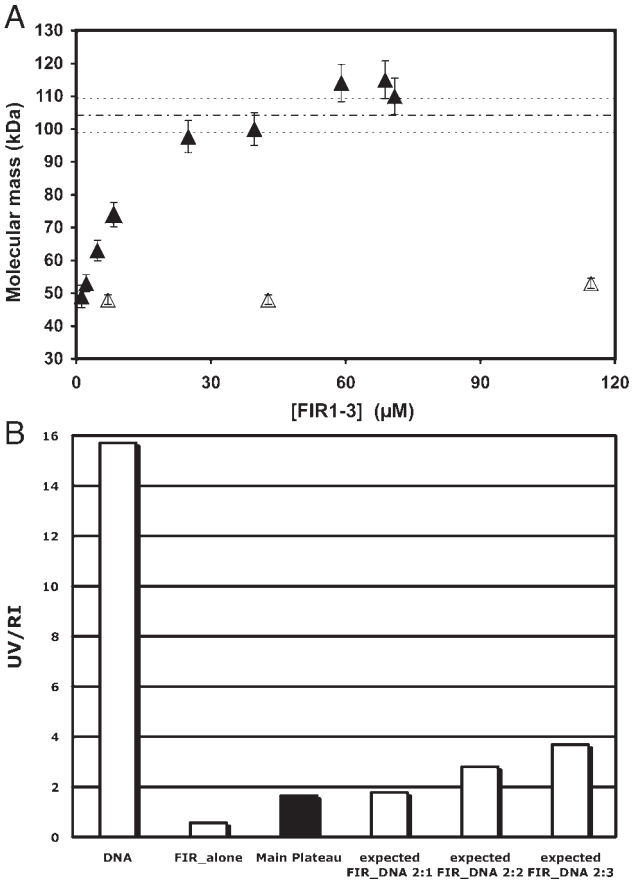


FIGURE 6: FUSE induces FIR dimerization. (A) FIR1−3 is analyzed alone and with an excess of FUSE27 (FUSE27:FIR1−3 molar ratio of > 1.1) by SEC-LS in 50 mM Tris-HCl, 150 mM NaCl, and 20 $\mu$M EDTA (pH 8.0). SEC elution peaks were detected by refractive index (RI) for masses of biomolecules and by static light scattering for molecular masses. Each triangle denotes an average molecular mass determined by static light scattering readings at a certain molecular concentration. Empty triangles represent the same data points for apo-FIR1−3 as in Figure 5B. Filled triangles represent the data points for average molecular masses determined at various concentrations of the FIR1-3-FUSE27 complex. The dashed line indicates the predicted molecular mass of 104.2 kDa for the complex of two FIR molecules and one FUSE27. The two dotted lines define the upper and lower bounds of the typical 5% standard errors from 104.2 kDa. The results indicate that FIR1−3 is monomeric in its apo form but dimerizes upon FUSE27 binding. Comparison with our previously published results for the FUSE-induced dimerization of FIR's two RRMs indicates that the two RRMs of FIR mediate its DNA-induced dimerization. (B) The UV:RI ratio of the FIR1−3−FUSE27 complex supports a 2:1 FIR:FUSE stoichiometry.

*Tripartite Interaction of the FUSE−FBP−FIR Complex*. To study the binding of the FUSE−FBP−FIR tripartite complex, we mixed 10 nM fluorescein-labeled FUSE53 and 2 $\mu$M full-length FBP with increasing concentrations of FIR 1−3. FBP (2 $\mu$M) was demonstrated in Figure 4 to be sufficient to specifically saturate 10 nM FUSE53. Reaction mixtures were incubated at room temperature for 30 min before fluorescence anisotropy was measured (Figure 9). The binding curves for the tripartite interactions were fit with two separate models of FIR stoichiometry in the tripartite complex: the first in which we assume that one FIR molecule binds to the FBP−FUSE complex

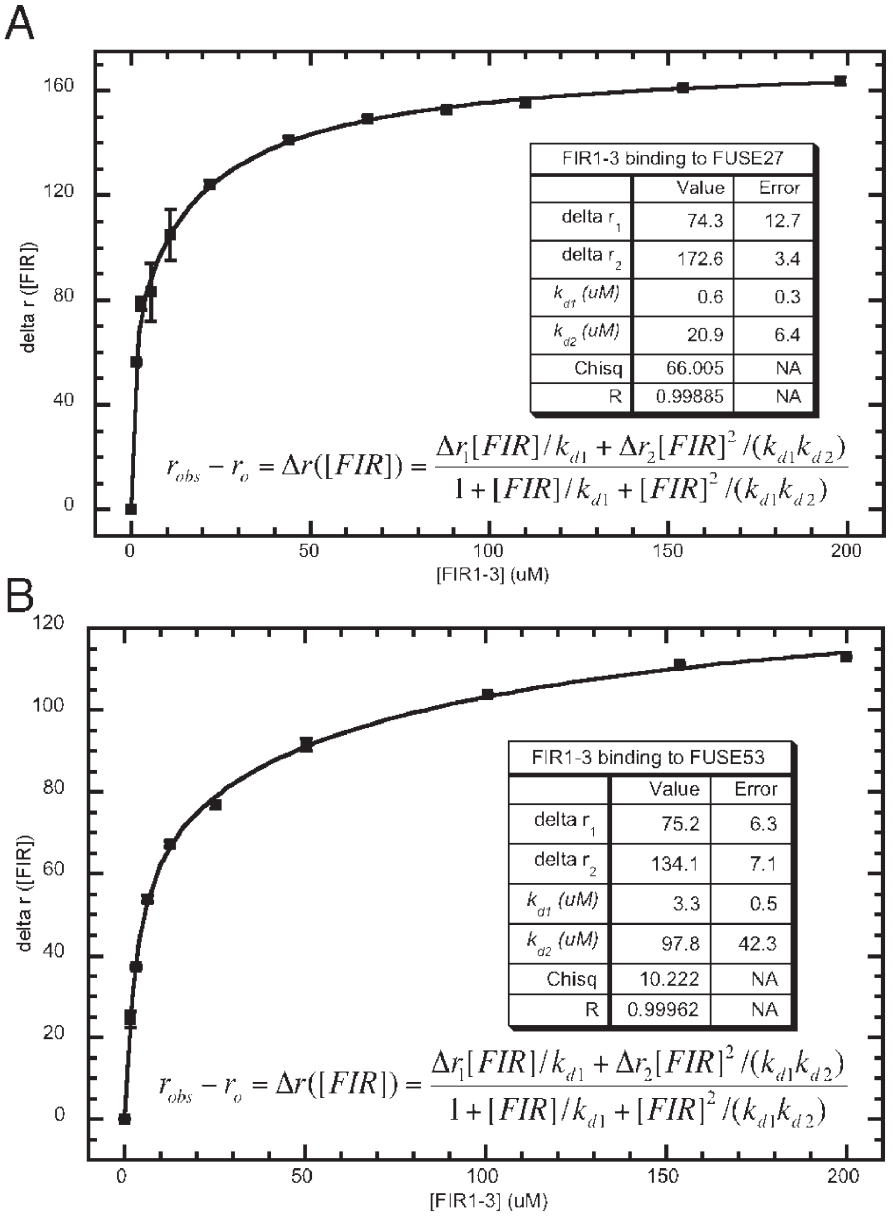


FIGURE 7: FIR binds to noncoding strand FUSE with dissociation constants in the low micromolar range. Fluorescein-labeled noncoding strand FUSE 27-mer (FUSE27) or 53-mer (FUSE53) at 10 nM was mixed with increasing concentrations of FIR1−3 and incubated at room temperature for 30 min before the measurement of fluorescence anisotropy. (A) FIR1−3 interacting with FUSE27. Fitting the binding curve with a two-site model reports two dissociation constants in the low micromolar range ($k_{d1} = 0.6 \pm 0.3\ \mu$M; $k_{d2} = 20.9 \pm 6.4\ \mu$M). (B) FIR1−3 interacting with FUSE53. Fitting with a two-site model estimates a pair of dissociation constants in the low micromolar range ($k_{d1} = 3.3 \pm 0.5\ \mu$M; $k_{d2} = 97.8 \pm 42.3\ \mu$M), which are similar to those of FIR1−3 interacting with FUSE27. The results indicate that FIR1−3 has a similar affinity for either FUSE27 or FUSE53 and binds more weakly to FUSE than FBP.

and the second in which we assume that two FIR molecules may bind the FBP−FUSE complex. In the fittings, we include the binding constants we derived for FBP to FUSE and FIR to FUSE in Figures 4 and 7. For the single-FIR model (model 1), we derived a $\chi^2$ of 88.387 and a dissociation constant for FIR binding to the FBP−FUSE complex ($k_d = 6.2 \pm 0.9\ \mu$M). For model 2, we derived a $\chi^2$ of 1.687 and two dissociation constants for binding of FIR to the FBP−FUSE complex ($k_{d1} = 2.2 \pm 0.2\ \mu$M; $k_{d2} = 156.2 \pm 31.5\ \mu$M). The two dissociation constants derived from model 2 are experimentally identical to those for the binding of FIR1−3 with FUSE53 in the absence of FBP. Model 2 was strongly preferred by the *F*-test ($F = 154.14$; $P < 0.0001$) and the corrected Akaike's Information Criteria (AICc) (Table 3). ΔAICc was −24.58 in favor of model 2, equivalent to a likelihood ratio of $> 2 \times 10^5$ in favor of the more complex model.

## DISCUSSION

*The Conformational Difference between the Melted DNA Strands May Contribute to FBP's Selective Binding to the Noncoding Strand of FUSE.* Upon *c-myc* transcription, FUSE is initially primed by chromatin-remolding complexes (*38*, *47*) and then melts into single-stranded DNA in response to the negative supercoiling forces propagated from the actions of the general transcription complex at the *c-myc* promoter region (*14*−*16*). The noncoding strand FUSE, with its deformable conformation, then serves as a mechano-sensing protein−DNA hinge to harness both FBP and FIR to fine-tune the progression of *c-myc* transcription (*11*, *15*, *38*, *40*, *48*). At the onset of the FBP-mediated regulation, FBP specifically binds only the noncoding strand, but not the coding strand or linear duplex FUSE (*10*, *17*, *38*). Our data suggest this strand preference may

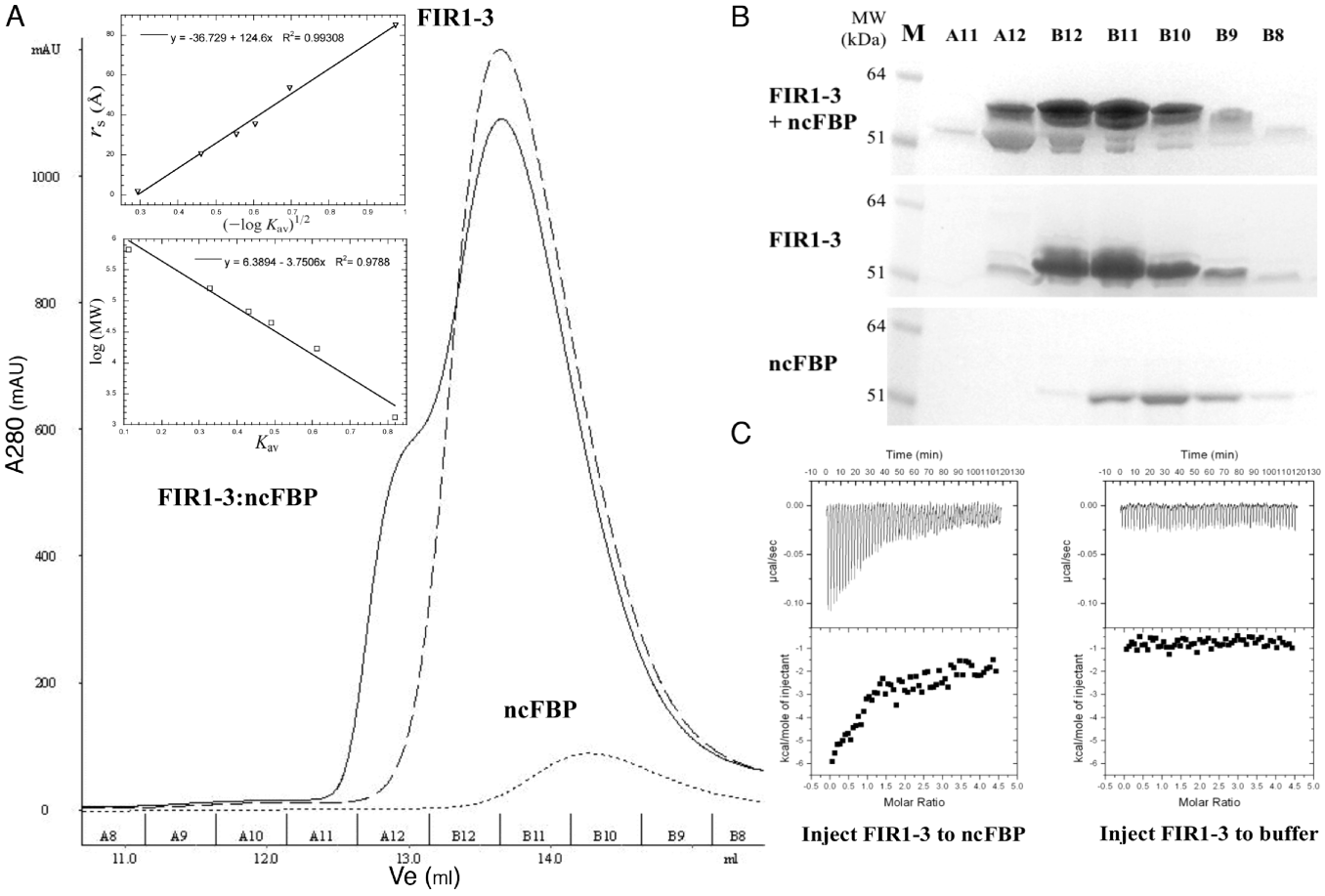


FIGURE 8: SEC peak shift caused by formation of the ncFBP−FIR1−3 complex verified by SDS−PAGE. ITC indicates weak association between FBP and FIR. (A) Analytical SEC of ncFBP and FIR1−3. ncFBP (8.3 nmol), FIR1−3 (66.6 nmol), or their mixture was subjected to the Superdex S-200, 10/30, GL SEC column. Elution traces were followed by their absorption at 280 nm. Standard calibration curves are displayed as embedded panels. The top inset shows the Stokes radius ($r_S$) plotted *vs* $(-\log K_{av})^{1/2}$; the bottom inset shows log(molecular mass) plotted *vs* $K_{av}$. The relative elution volume ($V_e$), estimated $r_S$, and apparent molecular mass for each population are listed in Table 2. (B) SDS−PAGE analysis of the SEC fractions. In the top panel, two proteins were present in fraction A12, the fraction that corresponds to the SEC peak shift. (C) ITC heat generation due to FBP−FIR association. The left panel shows heats generated via injection of 124.4 $\mu$M FIR1−3 into 6.4 $\mu$M ncFBP in the sample cell. Due to the weakness of association between ncFBP and FIR1−3, their dissociation constant could not be confidently determined, but was estimated to be beyond the single-digit micromolar range. The right panel shows the isothermal profile of injection of 124.4 $\mu$M FIR1−3 into buffer in the sample cell as a reference titration (see Materials and Methods for experimental conditions). Weak association between FBP and FIR in the absence of DNA is detected *in vitro*.

Table 2: SEC-Based Peak Analysis of FBP and FIR

| peak $V_e$[a] (mL) | assignment | predicted molecular mass (kDa) | apparent molecular mass (kDa) | estimated $r_S$[b] (Å) |
|---|---|---|---|---|
| 14.25 | ncFBP | 52.1 | 82.8 | 42.7 |
| 13.69 | FIR1−3 | 48.0 | 113.6 | 46.8 |
| ~13.00 | FIR1−3−ncFBP | 100.1 | ~167.6 | ~52.1 |

[a]Raw data drawn from analytical SEC-based analysis in Figure 8A. [b]$r_S$, Stokes radius.

be at least partially attributed to differences between the solution conformations of the coding and noncoding strands of FUSE. Both biochemical and structural characterizations reveal that FBP favors association with single-stranded DNA with minimal higher-order structure (*42*, *44*). We have found that as a single strand, the noncoding strand of FUSE takes one major conformational population in solution, which is extended as determined from its hydrodynamic radius (Table 1). This indicates that noncoding FUSE is mostly linear or extended when melted, which is a favored ssDNA conformation for FBP association. In contrast, roughly 50% of the coding strand FUSE population is in a compacted conformation as determined by its smaller hydrodynamic radius (Table 1). This suggests that the existence of secondary or tertiary structure in the coding strand of FUSE may impede FBP association.

Although the oligonucleotides we used here were synthetic and were not anchored on either end to mimic chromatin, our experiments demonstrate inherent sequence propensities for conformational populations for coding and noncoding FUSE. The conformational differences between the coding and noncoding FUSE suggest that upon FUSE melting, the coding strand becomes compact while the noncoding strand remains extended and linear, making its sequence freely available for the DNA−protein interactions required in the process.

*The Nonglobular Shape of FBP Is Consistent with a Previously Proposed Model in Which Its KH Domains May Be Linearly Aligned for Association with the Linear Noncoding FUSE.* Previously, a solution dynamics NMR study found the KH3 and KH4 domains of FBP to be linearly aligned in solution (*42*). All four KH domains of FBP are proposed to participate in the recognition of the linear noncoding strand of FUSE (*44*). We therefore studied the overall solution conformation of FBP with all of its KH domains. The apparent molecular mass (83 kDa) of ncFBP is 159% of its sequence-predicted

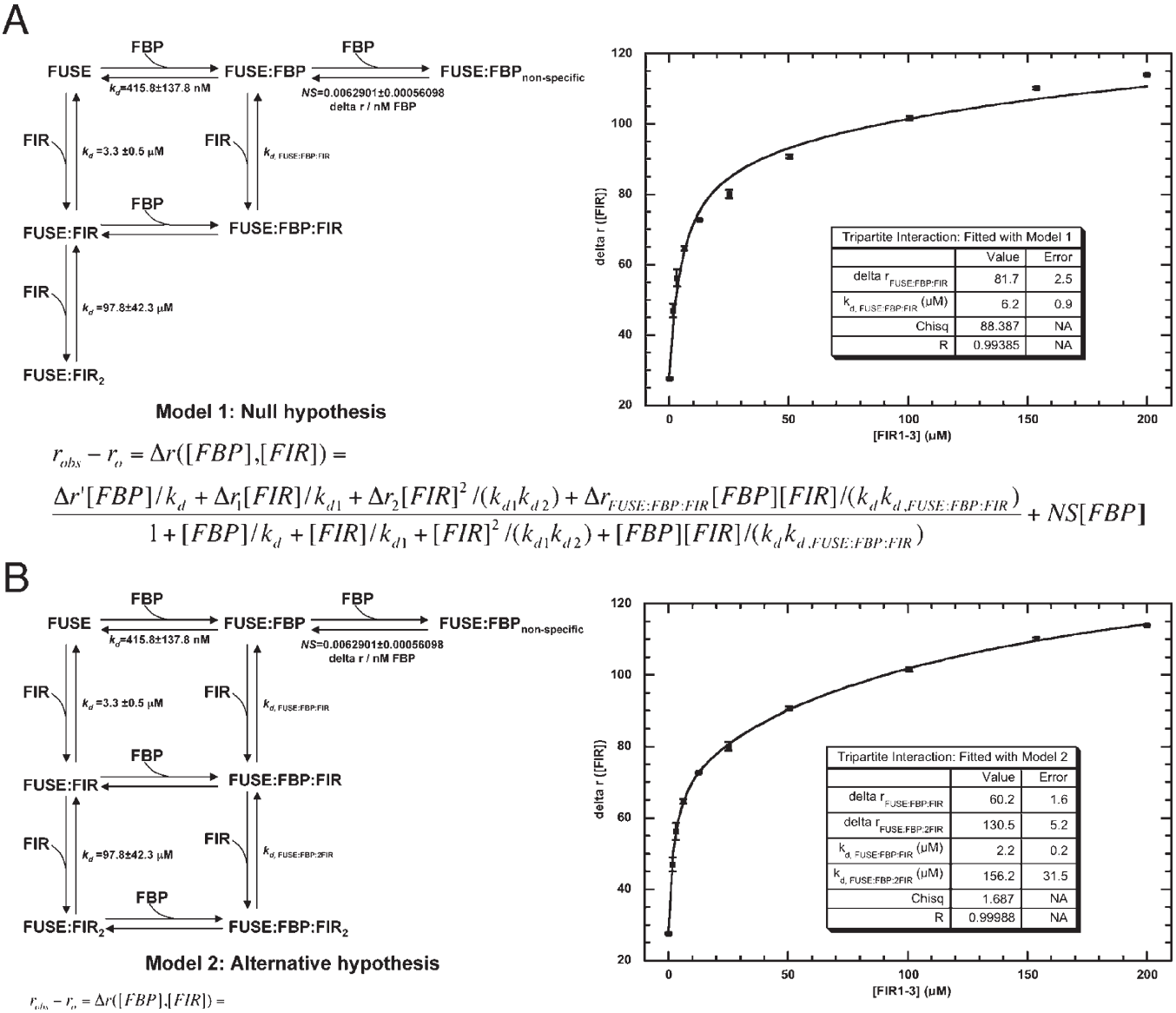


FIGURE 9: Tripartite interaction. Two FIR molecules can join the FBP−FUSE binary complex to form a $FIR_2$−FBP−FUSE quaternary complex. Fluorescein-labeled noncoding strand FUSE 53-mer (FUSE53, 10 nM) was mixed with 2 $\mu$M full-length FBP and increasing concentrations of FIR1−3. The reaction mixtures were incubated at room temperature for 30 min before measurement of their fluorescence anisotropy. The binding curves were fit with models based on two competing hypotheses for FIR binding to the FBP−FUSE binary complex. (A) Model 1. Null hypothesis, which assumes only one FIR molecule binds to the FBP−FUSE complex. A $k_d$ of 6.2 ± 0.9 $\mu$M is derived by fitting with the listed corresponding equation, with a $\chi^2$ of 88.387. (B) Model 2. Alternative hypothesis, which assumes two FIR molecules can bind to the FBP−FUSE complex. Two $k_d$ values (2.2 ± 0.2 and 156.2 ± 31.5 $\mu$M) are derived by fitting with the listed corresponding equation, with a $\chi^2$ of 1.687. Statistical analysis presented in Table 3 suggests that model 2 better describes the FIR−FBP−FUSE tripartite interaction, where two FIR molecules can join the FBP−FUSE complex to form a quaternary $FIR_2$−FBP−FUSE complex, with affinities experimentally identical to those for FIR binding to FUSE alone.

Table 3: Comparing Two Fitting Models

| | | | | Akaike's Information Criteria | | | *F*-test | |
|---|---|---|---|---|---|---|---|---|
| model[a] | SS[b] | no. of parameters[c] | DF[d] | AICc[e] | probability[f] | information ratio | $F^g$ | *P* value |
| 1 | 88.387 | 2 | 8 | 31.79 | 0.00% | 218093.70 | 154.14 | < 0.0001 |
| 2 | 1.687 | 4 | 6 | 7.21 | 100.00% | | | |

[a]Refer to Figure 9. Model 1, null hypothesis; model 2, alternative hypothesis. [b]Input information taken from Figure 9. SS, sum of squares. [c]Number of parameters in the corresponding fitting equation. [d]Degree of freedom. [e]Akaike's Information Criteria, corrected. [f]Probability model is correct. [g]*F* is the ratio of the percentage differences of the sums of squares and degrees of freedom between models 1 and 2.

molecular mass of 52 kDa, indicating a nonglobular shape, consistent with the hypothesis that all the FBP KH domains are linearly aligned in solution similar to the pattern seen for KH3 and KH4 (*42*). The linear arrangement of the FBP KH domains

and FUSE ssDNA target site implies that the favored association between the two may be partially facilitated by their conformational and/or structural fit.

*FBP Binds to FUSE with Nanomolar-Range Affinity*. We have for the first time reported a solution-based quantitative measurement of the affinity between FBP and FUSE (Figure 4) to complement previous study of FBP−FUSE binding by an electrophoretic mobility shift assay (EMSA) (*44*). The measurement of FBP's affinity for FUSE by two independent techniques yielded dissociation constants in the nanomolar range ($k_d$ = 415.8 ± 137.8 nM by FA, and $k_d$ = 168.6 ± 36.3 nM by FCS). This nanomolar-range affinity between FBP and FUSE may have reflected the participation of multiple KH domains of FBP in FUSE binding as mapped by Benjamin *et al.* (*44*). In summary, the outstanding features of the FBP−FUSE interaction include FBP's strong preference for a linear form of DNA and the participation of multiple FBP's modular KH domains (*42*, *44*). The directionality of FUSE binding for FBP is also mapped on the basis of the solution structure of the FBP KH3 and KH4 domains in complex with FUSE. KH4 is bound to the 5′ end, while KH3 is bound more toward the 3′ end of the FUSE DNA (*42*).

*FIR Is Monomeric in Solution but Dimerizes upon DNA Binding; DNA-Induced Dimerization Is Mediated by FIR's RRMs*. SEC-LS experiments demonstrate that FIR1−3 is monomeric in solution, though with a weak tendency to form higher-molecular mass aggregates at concentrations above 100 μM. Previously, the UHM domain of FIR was proposed to be responsible for the dimerization of FIR observed in SDS−PAGE (*28*). Later, Corsini *et al.* reported that FIR by itself is mostly monomeric in solution at 11 μM (*46*). Our observations in FIR1−3 correlate with Corsini *et al.*'s claim, and we have provided further experimental evidence illustrating that FIR1−3, which consists of both the carboxyl-terminal UHM and the two central RRMs, is predominantly monomeric in solution over a wide range of concentrations (Figure 5B). We have also studied the overall shape of FIR in solution. FIR1−3 has an apparent molecular mass of 114 kDa, which is 237% of its predicted molecular mass of 48 kDa, suggesting that the overall shape of FIR might highly deviate from the globular form (Table 2).

Solution-based SEC-LS studies further confirm that FIR1−3 undergoes DNA-induced dimerization in the presence of FUSE (Figure 6), an observation consistent with the FUSE-induced dimerization of FIR1+2 (*43*). These findings suggest that the two RRMs of FIR are the major structural motifs utilized for the protein's DNA-induced dimerization. The crystal structure of the FIR1+2−FUSE complex reveals a dimer interface between the two FIR subunits weakly stabilized by six hydrogen bonds which display nonideal geometry (*43*). This weak interface and the observation of the monomoric conformation of apo-FIR in solution suggest that the interaction of two protein monomers with a single strand of DNA is required to increase the local concentration of the protein and initiate FIR dimerization. Therefore, because of the passive dimerizing propensity of FIR, binding cooperativity is not expected, although two FIR monomers both associate with one DNA ligand. Biochemical characterization in combination with the crystal structure of the FIR1+2−FUSE complex also supports the fact that only RRM1 is used for DNA binding, while RRM2 is critical for the overall structure of FIR (*43*).

*Biophysical Data Suggest That Two FIR Molecules Bind FUSE Consecutively and Then Dimerize on FUSE via Their RRMs. Differential Affinities of FBP and FIR Implicate the Order of Complex Formation*. FIR binds to both the 53-mer and 27-mer of the noncoding FUSE sequence at comparable affinities in the micromolar range (for FIR1−3 and FUSE27, $k_{d1}$ = 0.6 ± 0.3 μM and $k_{d2}$ = 20.9 ± 6.4 μM; for FIR1−3 and FUSE53, $k_{d1}$ = 3.3 ± 0.5 μM and $k_{d2}$ = 97.8 ± 42.3 μM) (Figure 7), suggesting that the shorter nucleotide is sufficient for FUSE−FIR interaction and may be the region primarily responsible for interactions with FIR regulating transcription.

Via comparison of the equilibrium binding parameters of FIR1−3−FUSE association (Figure 7) with previously published dissociation constants for the association between FUSE and FIR1+2 (*43*), FIR's UHM does not significantly increase the affinity of the protein for FUSE DNA (Figure 7). This suggests that the two RRMs confer the majority of the DNA binding affinity of FIR. The role of FIR's UHM domain in the FBP−FIR−FUSE system remains unclear.

The curves for FIR−FUSE binding are fit with a model that assumes two FIR molecules may consecutively bind to FUSE to form a $FIR_2$−FUSE complex (Figure 7) (also see Equation Derivation in the Supporting Information). Our data suggest that there are two nonequivalent binding sites on FUSE for FIR binding and that FIR binds with a higher affinity for the first site and a lower affinity for the second (Figure 7). We propose that there may be two stages of FIR binding to FUSE. In the first stage, a FIR monomer binds DNA. In the second stage, as the concentration of FIR increases, a second FIR molecule joins to form a $FIR_2$−DNA complex. The lower-affinity stage may be the result of conformational changes in FUSE induced by the first FIR molecule, crowding over the available binding sites on FUSE for the second FIR, or structural changes in FIR needed to accommodate a dimer on FUSE. Therefore, no cooperativity is observed. This model is consistent with our observation of the concentration-dependent complex formation by SEC-LS analysis (Figure 6). In the SEC-LS study of FIR1+2, we also observed that "at a FIR1+2:H27 concentration of 4 μM the weight-average MW of the complex decreases to 30 kDa and the UV/RI ratio increase ~2-fold, suggesting that the FIR:DNA dissociation produces a 1:1 FIR:DNA complex as an intermediate in the FIR dimerization induced by DNA binding" (*43*). The crystal structure of FIR1+2 in complex with FUSE DNA (*43*) shows the dimeric conformation of FIR, where each FIR monomer uses only its RRM1, but not RRM2, to associate with a short tract of DNA. The canonical RNP of RRM2 is buried by FIR domain interactions. The amount of buried surface area between RRM1 and RRM2 (~2000 $Å^2$) is characteristic of obligate protein−protein interactions. Moreover, even for RRM1, its canonical RNP regions are not fully utilized for DNA binding, which in fact might lead to the low binding affinity of FIR for FUSE.

FIR binds FUSE53 at least 5-fold more weakly than FBP (Figures 4 and 7). The weaker affinity of FIR for FUSE, when compared with that of FBP and FUSE, suggests that, biochemically, lower cellular concentrations of FBP are required for FUSE association, which may provide a guiding mechanism for complex formation in the FUSE−FBP−FIR system.

*In Vivo Abundance of FBP and FIR*. FBP and FIR are abundant proteins in cells. The *in vivo* abundance of FBP and FIR in HeLa cells (estimated using the intensity of bands during Western blots) is determined to be 500000 molecules of FBP per cell and 250000 molecules of FIR per cell (unpublished data, D. Levens, National Cancer Institute, Bethesda, MD). If we estimate the volume of a nucleus to be 100−200 fL, the concentration of FBP in the nucleus is 5−10 μM and that of FIR is 2.5−5 μM.

These concentrations are well above the $k_d$ values measured for binding of FBP to FUSE (Figure 4) and near the values of the first $k_d$ for binding of FIR to FUSE (Figure 7). Given the short-lived nature of DNA base flipping and the opening and closing of DNA strands in solution, highly abundant proteins like FBP and FIR can hover near sites of transient opening (rather than rare proteins that would take time to find target sites to produce the requisite number of collisions necessary) to effect protein−DNA interactions.

*Weak FBP−FIR Association Exists in the Absence of DNA*. Do FBP and FIR interact with each other? Previously, Chung *et al*. detected the association of FBP and FIR indirectly using yeast two-hybrid techniques (*24*). Here, we use SEC to directly measure binding and find that FBP and FIR indeed associate *in vitro*. We also perform ITC analysis to study the affinity between FBP and FIR and qualitatively confirm FBP−FIR association, but the detailed dissociation constant of FBP with FIR cannot be confidently measured by ITC due to the low heat of generation and the weak affinity between the two entities (Figure 8). However, the lower bound of the dissociation constant for this interaction is estimated from our ITC data to be no stronger than tens of micromolar. The weak interaction between the proteins in the absence of FUSE is consistent with previous observations (*24*) and suggests that in the FUSE−FBP−FIR ternary complex (*25*), FBPs may have a positive but limited influence on FIR's binding affinity for FUSE. The affinity between FBP and FIR may fine-tune the transactivation effect of FBP, since tighter association with FIR is linked to weaker FBP transactivation (*24*). According to the literature, both FBP's amino-terminal and central domains are required for association with FIR (*24*, *25*).

*Tripartite FUSE−FBP−FIR Interaction: Two FIR Molecules May Join the FBP−FUSE Complex*. Previous *in vivo* observations demonstrate that following FUSE melting FBP binds to FUSE and facilitates promoter clearance. After a period of time, the FBP−FUSE complex is joined by the repressor FIR in a tripartite complex, from which FBP is ejected, and the FIR−FUSE complex forms a long-term repressive complex (*21*, *25*). Here, we show that FIR can bind as a dimer to the FBP−FUSE complex which is similar to the interaction of FIR with FUSE in the absence of FBP (Figure 9 and Table 3). The presence of FBP on FUSE slightly enhances the binding of the first FIR molecule; the $k_d$ values for the binding of the first FIR shifts from 3.3 ± 0.5 $\mu$M [FIR binding to FUSE only (Figure 7B)] to 2.2 ± 0.2 $\mu$M [FIR binding to the FBP−FUSE complex (Figure 9B)]. The enhanced affinity for FIR in the presence of FBP is consistent with EMSA experiments (*25*, *44*) and likely reflects the contribution of the weak FBP−FIR association (Figure 8C). Other $k_d$ values in the closed cycle of the FUSE−FBP−FIR interaction can be calculated to be 0.27 ± 0.10 $\mu$M for FBP binding the FUSE−FIR complex and 0.44 ± 0.27 $\mu$M for FBP binding the FUSE−$FIR_2$ complex (Figure 10).

*Real-Time Removal of FBP from FUSE: Potential Role of FUSE Conformation and Transcription-Generated Torsional Stress*. To remove the activator FBP from the FUSE−FBP−FIR system for *c-myc* regulation, the tRNA synthetase cofactor p38 could be regulated by either Parkin or MYC to target FBP for ubiquitination and eventual degradation (*11*, *32*, *49*). However, the protein degradation pathway has a turnover rate longer than what would be required for real-time feedback to the ongoing transcription event at the promoter site. For the mechanism behind the real-time removal of FBP from FUSE,

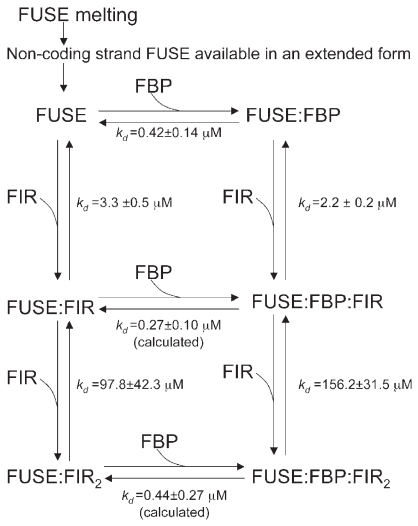


FIGURE 10: Scheme for FUSE−FBP−FIR interactions with quantitative annotations.

it was previously proposed that the DNA looping due to FIR dimerization might promote ejection of FBP (*43*).

Our new findings suggest that FIR dimerization itself is not sufficient to eject FBP from FUSE. First, the free energy for FBP−FUSE association is greater than the free energy released upon the second FIR molecule binding to FUSE and would therefore not energetically justify the replacement of FBP with FIR. According to our measurements based on FA, the free energy for FBP−FUSE association is −36.1 ± 0.8 kJ/mol, ~1.6-fold larger in magnitude than the free energy for the second FIR to bind to the FBP−FUSE complex (−22.7 ± 1.1 kJ/mol). Therefore, replacing FBP from FUSE with a second FIR molecule would not be thermodynamically feasible in the system. Second, the data for the FUSE−FBP−FIR tripartite interaction (Figure 9) also suggest that FIR dimerization does not eject FBP. Statistical analysis of the two mutually exclusive models (Table 3) favors the model in which two FIR molecules both can colocalize on FUSE with FBP.

Since we know FBP prefers binding to a linear form of FUSE DNA (*42*, *44*), while a FIR dimer favors a looped form of FUSE (*43*), a major energy barrier that exists to prevent FIR dimerization from ejecting FBP from FUSE would be the expense of entropy to transition from linear DNA to a looped conformation, which could significantly weaken FBP binding. In our *in vitro* setting, FIR dimerization itself is not energetically sufficient to eject FBP; an external energetic contribution is required. In the cell, we hypothesize that the dynamic torsional stress on the chromatin generated during active transcription might be the source of the driving force.

The major source of torsional stress in eukaryotes is transcription (*14*, *50*, *51*). DNA structure driven by supercoiling forces in general is known to participate in the regulation of genetic events, especially transcription (*37*, *52*−*54*). Especially for FUSE, the supercoiling forces not only contribute to its melting (*10*, *11*, *15*, *16*) but also may modulate FUSE conformation to dynamically communicate the progression of transcription to the upstream FUSE−FBP−FIR regulatory system (*11*, *15*, *16*, *38*). The transition from a FBP-dominant to a FIR-dominant control happens mainly during the promoter escape stage of transcription (*21*). During promoter escape, the action (*55*) of the RNA polymerase (*15*) and associated general transcription factors,

particularly the wrenching activity by TFIIH (*39*, *56*) on the chromatin, may generate dynamic torque sufficient to drive upstream FUSE DNA into a looped form, preventing FBP binding, but retaining FIR (Figure 11E,F). Therefore, we hypothesize that the continuing dynamic torsional stress on the chromatin during transcription might contribute to the real-time displacement of FBP from FUSE.

*Model for FUSE−FBP−FIR Complex-Mediated c-myc Regulation*. Our characterization of interactions of FBP and FIR with FUSE allows us to further understand the physical basis behind the FUSE−FBP−FIR system for the transcriptional regulation of *c-myc* (Figure 11). After the transcription-induced torsional stress on the chromatin leads to the melting of FUSE (*14*−*16*), the coding strand of FUSE tends to compact itself and thus blocks its accessibility from FBP, while the noncoding strand stays in an extended form (Figures 3 and 11B), a preferred DNA conformation for FBP association (*42*, *44*). During transcription initiation (*21*), FBP binds to the underwound, linear noncoding strand of FUSE (*10*, *42*, *44*) (Figure 11C) with a nanomolar-range dissociation constant (Figures 4 and 10). The stronger binding between FBP and FUSE versus that between FIR and FUSE helps prioritize association of FBP with FUSE (Figures 4 and 7). The carboxyl terminus of FBP points toward the 5′ end of the noncoding FUSE (*42*) and may present FBP's C-terminal activation domain (AD) to the p89 subunit of TFIIH (*21*), thereby upregulating *c-myc* transcription during both transcription initiation and promoter escape (*21*) (Figure 11C). During promoter escape (*21*), the presence of FBP on FUSE helps recruit the first FIR molecule, probably through FBP's central and N-terminal domains (*24*, *25*). With increasing concentrations of FIR, a second FIR molecule may join to form a quaternary complex consisting of FUSE, FBP, and FIR (*25*) (Figure 9B and Table 3). FIR may use its N-terminal repression domain to compete FBP's AD away from contacting p89 and thus cancel FBP's activating effect by locking TFIIH in an activation-resistant state, while still allowing the basal levels of transcription (*25*) (Figure 11D−F). At a later stage of promoter escape, an additional energetic source, likely the continuing dynamic torque generated during active transcription, may loop FUSE, thereby ejecting FBP but retaining FIR, likely in its dimeric form (*43*) (Figures 7B and Figure 11E,F). The eventual ejection of FIR from FUSE is likely due to the reannealing of FUSE in later stages of transcription (Figure 11F−A). Our *in vitro* study, with an assumption that FUSE, FBP, and FIR behave similarly *in vivo*, supplements previous observations to reveal that FUSE, FBP, and FIR form a system in which the conformation of a remote *cis* component (FUSE) mechanically senses the supercoiling forces (*15*, *16*) generated by a genetic event (transcription) (*15*, *16*, *38*, *40*) and coordinates *trans* effectors (FBP and FIR) to regulate transcription by influencing the general transcription machinery (TFIIH) (*39*, *56*) in real time to fine-tune the expression of an essential proto-oncogene, *c-myc* (*11*, *57*, *58*). We propose the contribution of the dynamic torsional force in the structural transition of the FUSE−FBP−FIR complex on the basis of our observation of the insufficiency of FIR dimerization to eject FBP, and the understanding of the prevalence of torsional forces existing in transcriptional events in cells. Further biological and biophysical experiments will be needed to determine if the unusual mode of transcriptional control by the FBP−FIR−FUSE system is unique to the essential transcription factor *c-myc* or is a broadly used mechanism in biology for the regulation of critical genetic events (*10*, *14*, *41*, *59*).

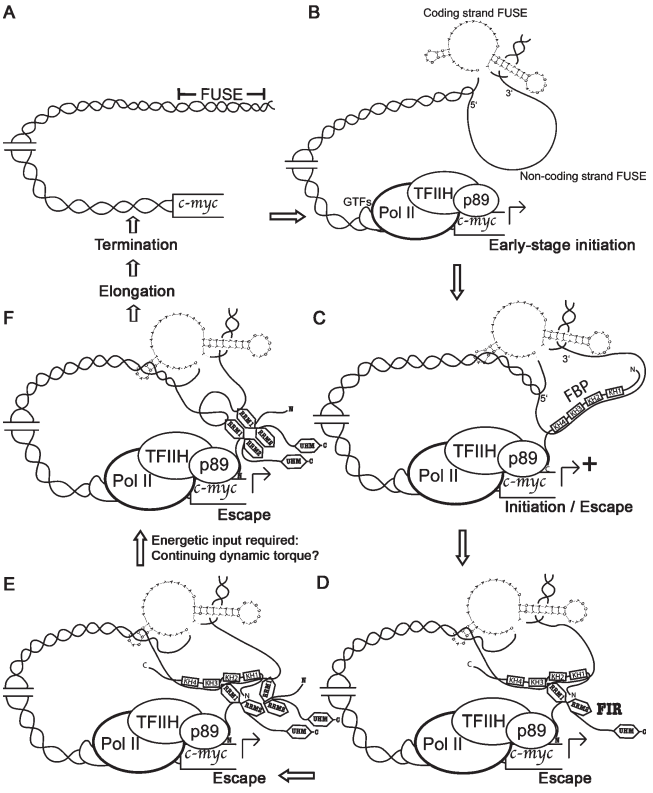


FIGURE 11: Revised model for the FUSE−FBP−FIR complex-mediated regulation of *c-myc* transcription. Additional descriptions based on our observation of the interactions among FUSE, FBP, and FIR supplement the existing knowledge of the FUSE−FBP−FIR system. In this model, we have assumed that FUSE, FBP, and FIR interact similarly in a cell and in our *in vitro* system. (A) FUSE is an AT-rich region of the chromatin ~1.7 kb upstream of the P2 start site of the *c-myc* oncogene. (B) Upon active transcription (likely during the early stage initiation), FUSE melts into single-stranded DNA in response to the torsional stress on the chromatin. The coding strand of FUSE has an intrinsic tendency to form secondary or tertiary structures, while the melted noncoding strand of FUSE is extended, a favored conformation for FBP association. GTFs stands for general transcription factors (*55*, *60*). (C) The activator FBP binds to the linear noncoding strand of FUSE with FBP's central DNA binding domain consisting of four KH motifs. The C-terminal activation domain of FBP contacts the p89 subunit of TFIIH and upregulates *c-myc* transcription. (D) As the transcription progresses, the repressor FIR joins the FUSE−FBP activation complex to form a ternary repression complex (FUSE−FBP−FIR). The N-terminal repression domain of FIR may displace the C-terminal activation domain of FBP from p89. FBP-mediated upregulation of *c-myc* transcription is canceled, while the basal transcription continues. (E) A second molecule of FIR can join the FUSE−FBP−FIR ternary complex to form a FUSE−FBP−$FIR_2$ quaternary complex for transitioning into the next stage of complex formation. (F) An energetic input may be required to change the conformation of FUSE and therefore eject FBP. This energetic contribution is likely to come from the torque on the chromatin generated by the continuing progression of transcription. The torque may wrench the noncoding FUSE away from linearity into a looped form, to which FBP can no longer bind, but a preferred form of FUSE for FIR association. For the path from panel F to panel A, eventually the termination of transcription releases the torsional stress on chromatin. FUSE is reannealed into a DNA double helix. FIR is ejected from FUSE due to the loss of the single-stranded nature of FUSE.

## ACKNOWLEDGMENT

We thank Dr. David Levens and his group member Dr. Juhong Liu at the National Cancer Institute for their gifts of the FBP and FIR plasmids and their highly informative discussions. We also thank Dr. Janie Merkel and Mr. Michael Salcius at the Yale

University Small Molecule Discovery Center for their technical assistance.

## SUPPORTING INFORMATION AVAILABLE

Detailed description of the methodologies used in this study. This material is available free of charge via the Internet at http://pubs.acs.org.

## REFERENCES


1. Marcu, K. B., Bossone, S. A., and Patel, A. J. (1992) *myc* function and regulation. *Annu. Rev. Biochem. 61*, 809–860.
2. Secombe, J., Pierce, S. B., and Eisenman, R. N. (2004) Myc: A weapon of mass destruction. *Cell 117*, 153–156.
3. Trumpp, A., Refaeli, Y., Oskarsson, T., Gasser, S., Murphy, M., Martin, G. R., and Bishop, J. M. (2001) c-Myc regulates mammalian body size by controlling cell number but not cell size. *Nature 414*, 768–773.
4. de la Cova, C., Abril, M., Bellosta, P., Gallant, P., and Johnston, L. A. (2004) *Drosophila* myc regulates organ size by inducing cell competition. *Cell 117*, 107–116.
5. Grandori, C., Cowley, S. M., James, L. P., and Eisenman, R. N. (2000) The Myc/Max/Mad network and the transcriptional control of cell behavior. *Annu. Rev. Cell Dev. Biol. 16*, 653–699.
6. Levens, D. (2002) Disentangling the MYC web. *Proc. Natl. Acad. Sci. U.S.A. 99*, 5757–5759.
7. Levens, D. L. (2003) Reconstructing MYC. *Genes Dev. 17*, 1071–1077.
8. Kelly, K., and Siebenlist, U. (1986) The regulation and expression of *c-myc* in normal and malignant cells. *Annu. Rev. Immunol. 4*, 317–338.
9. Spencer, C. A., and Groudine, M. (1991) Control of *c-myc* regulation in normal and neoplastic cells. *Adv. Cancer Res. 56*, 1–48.
10. Michelotti, G. A., Michelotti, E. F., Pullner, A., Duncan, R. C., Eick, D., and Levens, D. (1996) Multiple single-stranded *cis* elements are associated with activated chromatin of the human *c-myc* gene *in vivo*. *Mol. Cell. Biol. 16*, 2656–2669.
11. Chung, H.-J., and Levens, D. (2005) *c-myc* Expression: Keep the Noise Down. *Mol. Cells 20*, 157–166.
12. Liu, J., and Levens, D. (2006) Making Myc. In The Myc/Max/Mad Transcription Factor Network (Eisenman, R. N., Ed.) pp 1−32, Springer-Verlag, Berlin.
13. Avigan, M. I., Strober, B., and Levens, D. (1990) A far upstream element stimulates *c-myc* expression in undifferentiated leukemia cells. *J. Biol. Chem. 265*, 18538–18545.
14. Levens, D., Duncan, R. C., Tomonaga, T., Michelotti, G. A., Collins, I., Davis-Smyth, T., Zheng, T., and Michelotti, E. F. (1997) DNA conformation, topology, and the regulation of c-myc expression. *Curr. Top. Microbiol. Immunol. 224*, 33–46.
15. Kouzine, F., Liu, J., Sanford, S., Chung, H.-J., and Levens, D. (2004) The dynamic response of upstream DNA to transcription-generated torsional stress. *Nat. Struct. Mol. Biol. 11*, 1092–1100.
16. He, L. S., Liu, J. H., Collins, I., Sanford, S., O'Connell, B., Benham, C. J., and Levens, D. (2000) Loss of FBP function arrests cellular proliferation and extinguishes *c-myc* expression. *EMBO J. 19*, 1034–1044.
17. Duncan, R., Bazar, L., Michelotti, G., Tomonaga, T., Krutzsch, H., Avigan, M., and Levens, D. (1994) Sequence-specific, single-strand binding-protein activates the far upstream element of *c-myc* and defines a new DNA-binding motif. *Genes Dev. 8*, 465–480.
18. Bazar, L., Harris, V., Sunitha, I., Hartmann, D., and Avigan, M. (1995) A transactivator of *c-myc* is coordinately regulated with the proto-oncogene during cellular growth. *Oncogene 10*, 2229–2238.
19. Bazar, L., Meighen, D., Harris, V., Duncan, R., Levens, D., and Avigan, M. (1995) Targeted melting and binding of a DNA regulatory element by a transactivator of *c-myc*. *J. Biol. Chem. 270*, 8241–8248.
20. Davis-Smyth, T., Duncan, R. C., Zheng, T., Michelotti, G., and Levens, D. (1996) The far upstream element-binding proteins comprise an ancient family of single-strand DNA-binding transactivators. *J. Biol. Chem. 271*, 31679–31687.
21. Liu, J. H., Akoulitchev, S., Weber, A., Ge, H., Chuikov, S., Libutti, D., Wang, X. W., Conaway, J. W., Harris, C. C., Conaway, R. C., Reinberg, D., and Levens, D. (2001) Defective interplay of activators and repressors with TFIIH in xeroderma pigmentosum. *Cell 104*, 353–363.
22. Duncan, R., Collins, I., Tomonaga, T., Zhang, T., and Levens, D. (1996) A unique transactivation sequence motif is found in the carboxyl-terminal domain of the single-strand-binding protein FBP. *Mol. Cell. Biol. 16*, 2274–2282.
23. He, L., Weber, A., and Levens, D. (2000) Nuclear targeting determinants of the far upstream element binding protein, a c-myc transcription factor. *Nucleic Acids Res. 28*, 4558–4565.
24. Chung, H.-J., Liu, J., Dundr, M., Nie, Z., Sanford, S., and Levens, D. (2006) FBPs are calibrated molecular tools to adjust gene expression. *Mol. Cell. Biol. 26*, 6584–6597.
25. Liu, J. H., He, L. S., Collins, I., Ge, H., Libutti, D., Li, J. F., Egly, J. M., and Levens, D. (2000) The FBP interacting repressor targets TFIIH to inhibit activated transcription. *Mol. Cell 5*, 331–341.
26. Maris, C., Dominguez, C., and Allain, F. H. (2005) The RNA recognition motif, a plastic RNA-binding platform to regulate post-transcriptional gene expression. *FEBS J. 272*, 2118–2131.
27. Kielkopf, C. L., Lucke, S., and Green, M. R. (2004) U2AF homology motifs: Protein recognition in the RRM world. *Genes Dev. 18*, 1513–1526.
28. Page-McCaw, P. S., Amonlirdviman, K., and Sharp, P. A. (1999) PUF60: A novel U2AF65-related splicing activity. *RNA 5*, 1548–1560.
29. Hu, Y., Holloway, A. J., and Bowtell, D. D. L. (1996) Interaction of sina and siah ring finger proteins with proteins involved in RNA metabolism, detected using the yeast two hybrid system. Submitted (March 1996) to the EMBL/GenBank/DDBJ databases.
30. Bouffard, P., Barbar, E., Briere, F., and Boire, G. (2000) Interaction cloning and characterization of RoBPI, a novel protein binding to human Ro ribonucleoproteins. *RNA 6*, 66–78.
31. Wang, X., Avigan, M., and Norgren, R. B., Jr. (1998) FUSE-binding protein is developmentally regulated and is highly expressed in mouse and chicken embryonic brain. *Neurosci. Lett. 252*, 191–194.
32. Ko, H. S., Kim, S. W., Sriram, S. R., Dawson, V. L., and Dawson, T. M. (2006) Identification of far upstream element-binding protein-1 as an authentic Parkin substrate. *J. Biol. Chem. 281*, 16193–16196.
33. Matsushita, K., Tomonaga, T., Shimada, H., Shioya, A., Higashi, M., Matsubara, H., Harigaya, K., Nomura, F., Libutti, D., Levens, D., and Ochiai, T. (2006) An essential role of alternative splicing of *c-myc* suppressor FUSE-binding protein-interacting repressor in carcinogenesis. *Cancer Res. 66*, 1409–1417.
34. Matsushita, K., Tomonaga, T., Kajiwara, T., Shimada, H., Itoga, S., Hiwasa, T., Kubo, S., Ochiai, T., Matsubara, H., and Nomura, F. (2009) *c-myc* suppressor FBP-interacting repressor for cancer diagnosis and therapy. *Front. Biosci. 14*, 3401–3408.
35. Huth, J. R., Yu, L., Collins, I., Mack, J., Mendoza, R., Isaac, B., Braddock, D. T., Muchmore, S. W., Comess, K. M., Fesik, S. W., Clore, G. M., Levens, D., and Hajduk, P. J. (2004) NMR-driven discovery of benzoylanthranilic acid inhibitors of far upstream element binding protein binding to the human oncogene c-myc promoter. *J. Med. Chem. 47*, 4851–4857.
36. Tomonaga, T., and Levens, D. (1996) Activating transcription from single stranded DNA. *Proc. Natl. Acad. Sci. U.S.A. 93*, 5830–5835.
37. Rothman-Denes, L. B., Dai, X., Davydova, E., Carter, R., and Kazmierczak, K. (1998) Transcriptional regulation by DNA structural transitions and single-stranded DNA-binding proteins. *Cold Spring Harbor Symp. Quant. Biol. 63*, 63–73.
38. Liu, J., Kouzine, F., Nie, Z., Chung, H.-J., Elisha-Feil, Z., Weber, A., Zhao, K., and Levens, D. (2006) The FUSE/FBP/FIR/TFIIH system is a molecular machine programming a pulse of *c-myc* expression. *EMBO J. 25*, 2119–2130.
39. Weber, A., Liu, J., Collins, I., and Levens, D. (2005) TFIIH operates through an expanded proximal promoter to fine-tune c-myc expression. *Mol. Cell. Biol. 25*, 147–161.
40. Kouzine, F., Sanford, S., Elisha-Feil, Z., and Levens, D. (2008) The functional response of upstream DNA to dynamic supercoiling *in vivo*. *Nat. Struct. Mol. Biol. 15*, 146–154.
41. Kouzine, F., and Levens, D. (2007) Supercoil-driven DNA structures regulate genetic transactions. *Front. Biosci. 12*, 4409–4423.
42. Braddock, D. T., Louis, J. M., Baber, J. L., Levens, D., and Clore, G. M. (2002) Structure and dynamics of KH domains from FBP bound to single-stranded DNA. *Nature 415*, 1051–1056.
43. Crichlow, G. V., Zhou, H., Hsiao, H. H., Frederick, K. B., Debrosse, M., Yang, Y., Folta-Stogniew, E. J., Chung, H.-J., Fan, C., De la Cruz, E. M., Levens, D., Lolis, E., and Braddock, D. (2008) Dimerization of FIR upon FUSE DNA binding suggests a mechanism of *c-myc* inhibition. *EMBO J. 27*, 277–289.
44. Benjamin, L. R., Chung, H.-J., Sanford, S., Kouzine, F., Liu, J., and Levens, D. (2008) Hierarchical mechanisms build the DNA-binding specificity of FUSE binding protein. *Proc. Natl. Acad. Sci. U.S.A. 105*, 18296–18301.
45. Folta-Stogniew, E., and Williams, K. R. (1999) Determination of molecular masses of proteins in solution: Implementation of an HPLC size exclusion chromatograpy and laser light scattering service in a core laboratory. *J. Biomol. Technol. 10*, 51–63.

46. Corsini, L., Hothorn, M., Stier, G., Rybin, V., Scheffzek, K., Gibson, T. J., and Sattler, M. (2009) Dimerization and protein binding specificity of the U2AF homology motif of the splicing factor Puf60. *J. Biol. Chem. 284*, 630–639.
47. Liu, H., Kang, H., Liu, R., Chen, X., and Zhao, K. (2002) Maximal induction of a subset of interferon target genes requires the chromatin remodeling activity of the BAF complex. *Mol. Cell. Biol. 22*, 6471–6479.
48. Tomonaga, T., Michelotti, G. A., Libutti, D., Uy, A., Sauer, B., and Levens, D. (1998) Unrestraining genetic processes with a protein-DNA hinge. *Mol. Cell 1*, 759–764.
49. Kim, M. J., Park, B.-J., Kang, Y.-S., Kim, H. J., Park, J.-H., Kang, J. W., Lee, S. W., Han, J. M., Lee, H.-W., and Kim, S. (2003) Downregulation of FUSE-binding protein and *c-myc* by tRNA synthetase cofactor p38 is required for lung cell differentiation. *Nat. Genet. 34*, 330–336.
50. Cozzarelli, N. R., and Wang, J. C. (1990) DNA topology and its biological effects, Cold Spring Harbor Laboratory Press, Plainview, NY.
51. Freeman, L. A., and Garrard, W. T. (1992) DNA supercoiling in chromatin structure and gene expression. *Crit. Rev. Eukaryotic Gene Expression 2*, 165–209.
52. Dai, X., and Rothman-Denes, L. B. (1999) DNA structure and transcription. *Curr. Opin. Microbiol. 2*, 126–130.
53. Dai, X., Greizerstein, M. B., Nadas-Chinni, K., and Rothman-Denes, L. B. (1997) Supercoil-induced extrusion of a regulatory DNA hairpin. *Proc. Natl. Acad. Sci. U.S.A. 94*, 2174–2179.
54. Collins, I., Weber, A., and Levens, D. (2001) Transcriptional consequences of topoisomerase inhibition. *Mol. Cell. Biol. 21*, 8437–8451.
55. Chen, H.-T., and Hahn, S. (2004) Mapping the location of TFIIB within the RNA polymerase II transcription preinitiation complex: A model for the structure of the PIC. *Cell 119*, 169–180.
56. Kim, T.-K., Ebright, R. H., and Reinberg, D. (2000) Mechanism of ATP-dependent promoter melting by transcription factor IIH. *Science 288*, 1418–1421.
57. Strobl, L. J., and Eick, D. (1992) Hold back of RNA polymerase II at the transcription start site mediates down-regulation of *c-myc in vivo*. *EMBO J. 11*, 3307–3314.
58. Krumm, A., Hickey, L. B., and Groudine, M. (1995) Promoter-proximal pausing of RNA polymerase II defines a general rate-limiting step after transcription initiation. *Genes Dev. 9*, 559–572.
59. Miller, A., Dai, X., Choi, M., Glucksmann-Kuis, M. A., and Rothman-Denes, L. B. (1996) Single-stranded DNA-binding proteins as transcriptional activators. *Methods Enzymol. 274*, 9–20.
60. Esnault, C., Ghavi-Helm, Y., Brun, S., Soutourina, J., Van Berkum, N., Boschiero, C., Holstege, F., and Werner, M. (2008) Mediator-dependent recruitment of TFIIH modules in preinitiation complex. *Mol. Cell 31*, 337–346.